

# Higgs Quantum Numbers in Weak Boson Fusion

Christoph Englert,<sup>1</sup> Dorival Gonçalves-Netto,<sup>2</sup> Kentarou Mawatari,<sup>3</sup> and Tilman Plehn<sup>2</sup>

<sup>1</sup>*IPPP, Department of Physics, Durham University, United Kingdom*

<sup>2</sup>*Institut für Theoretische Physik, Universität Heidelberg, Germany*

<sup>3</sup>*Theoretische Natuurkunde and IIHE/ELEM, Vrije Universiteit Brussel  
and International Solvay Institutes, Brussels, Belgium*

Recently, the ATLAS and CMS experiments have reported the discovery of a Higgs like resonance at the LHC. The next analysis step will include the determination of its spin and CP quantum numbers or the form of its interaction Lagrangian channel-by-channel. We show how weak-boson-fusion Higgs production and associated  $ZH$  production can be used to separate different spin and CP states.

## Contents

<b>I. Introduction</b>	2
<b>II. Kinematics</b>	2
A. Flipped Nelson	3
B. Hadron collider observables	5
C. Contaminating sub-processes	7
<b>III. Lagrangian</b>	8
A. Spin zero	9
B. Spin one	9
C. Spin two	10
<b>IV. Analysis</b>	11
A. Tagging jet kinematics	12
B. Higgs-jet correlations	14
C. Including Higgs decays	15
D. Basic strategy	16
E. Comparison of observables	16
<b>V. <math>ZH</math> production</b>	18
<b>VI. Outlook</b>	19
<b>Acknowledgments</b>	20
<b>Complete set of observables</b>	21
<b>References</b>	24

## I. INTRODUCTION

Recently, ATLAS and CMS have reported the discovery of a Higgs-like [1] resonance with a mass around 126 GeV [2, 3]. Decays to  $\gamma\gamma$ ,  $ZZ^*$ ,  $WW^*$ , and recently  $\tau\tau$  [4, 5] have been established, with coupling strengths consistent with the Standard Model [6–8]. While this ‘Higgs discovery’ is a great triumph for experimental and theoretical high energy physics, the detailed study of this new state will require many years of work at the LHC and possibly a future linear collider.

The ultimate goal of such studies will be a term-by-term and channel-by-channel confirmation of the structure of the Higgs Lagrangian from data. If we assume that the observed resonance is indeed responsible for electroweak symmetry breaking the leading renormalized operators describing the couplings to all massive fermions and gauge bosons are fixed. In an effective theory approach higher-dimensional operators will induce additional (anomalous) Higgs couplings, which can be constrained from measurements [9]. Some of these higher-dimensional operators are responsible for the most striking LHC observables — Higgs production in gluon fusion and Higgs decays to photons. Both of these operators have mass dimension six before and five after electroweak symmetry breaking, but they are not suppressed by a large mass scale. In the presence of Yukawa couplings both, fermion and massive gauge boson loops induce higher-dimensional operators suppressed by powers of  $v$  [10].

This structure of higher-dimensional operators suggests that we should have a careful look at the structure of operators responsible for the observation of the new ‘Higgs’ resonance [11, 12]. Only after the operator basis is fixed we can determine the corresponding couplings. In that sense the current coupling extractions [6–8] rely on strong assumptions about the structure of the Higgs Lagrangian or the Higgs couplings.

The structure of the Higgs Lagrangian is strongly linked to, but not entirely equivalent to the spin and quantum numbers of the heavy resonance. An example is the tensor structure of a coupling of a CP-even scalar to two  $W$  bosons, which can be constructed using the gauge field or the field strength tensor. Only the first can generate a mass for the  $W$  boson and unitarize the longitudinal Goldstone boson scattering. It is well known how to distinguish between different coupling structures, using the Cabibbo–Maksymowicz–Dell’Aquila–Nelson [13, 14] angles in fully reconstructed  $X \rightarrow ZZ$  decays [5, 15–19]. We will show in this paper that an equivalent way of determining the Higgs coupling structure can be based on weak-boson-fusion (WBF) events [11, 12, 20–22]. The two methods nicely complement each other, covering a wide range of production and decay channels [23]. In addition, we will show how the angular  $H \rightarrow ZZ$  analysis can be applied to associated  $ZH$  production with a fully reconstructed decay  $H \rightarrow b\bar{b}$  [24].

In contrast to these two complete methods based on a full set of angular correlations, the determination of coupling structures for example from  $X \rightarrow \gamma\gamma$  events is somewhat limited [25]. The same channel makes it unlikely that the set of ‘Higgs’ measurements is due to a spin-1 resonance, which cannot decay to two neutral gauge bosons because of the Landau–Yang theorem [26]. Nevertheless, we will see that there is a case for a dedicated channel-by-channel LHC study, carefully keeping track of implicit assumptions for example when testing spin-2 models with and without form factor corrections.

In this paper we develop a complete strategy to extract the structure of the ‘Higgs’ operators in weak boson fusion. We start by constructing the appropriate observables and linking them to the  $X \rightarrow ZZ$  angles. We then define the operator basis best suited for weak boson fusion, which is slightly different from the basis used for Higgs decays. In the second part of the paper we study jet-jet and jet- $X$  correlations. We show that the set of them is sufficient to probe our set of coupling operators and compare the individual distinguishing power for the most popular coupling structures. Finally, we add brief comment on the angular correlation in associated  $ZX$  production, with a hadronic decay  $X \rightarrow b\bar{b}$ .

## II. KINEMATICS

Before we can develop a detailed strategy on how to extract the form of the Higgs interaction Lagrangian at the LHC we need to define our theoretical framework, our set of observables, and their relation for example to the well-known  $H \rightarrow ZZ$  analysis. The latter is usually formulated in terms of a set of angles, where the angle between the two  $Z$  decay planes is one of the most promising observables. It is proto-typical for linking the measurement of quantum numbers or Lagrangian operators to angular correlations, leaving any kind of rate measurement for an unbiased determination of the corresponding coupling strength. The same approach we suggest for an angular analysis of weak boson fusion Higgs events. As we will see below, weak boson fusion will offer one additional handle in form of transverse momentum or energy spectra, but its analysis requires some care in its interpretation.

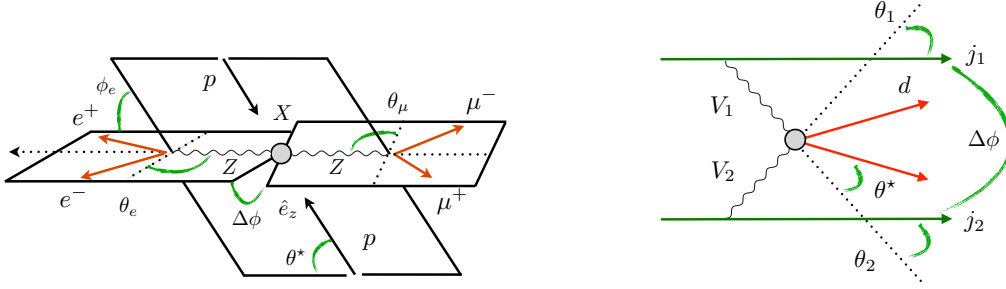


Figure 1: Kinematic setup for the angular analysis of  $H \rightarrow ZZ$  events (left) and Higgs events in WBF production (right). All angles are defined in Eq.(2) and Eq.(4).

### A. Flipped Nelson

The ‘traditional’ observables to measure the coupling structure of a massive state decaying to two weak gauge bosons are the Cabibbo–Maksymowicz–Dell’Aquila–Nelson [13, 14] angles. The kinematics for the decay  $X \rightarrow ZZ \rightarrow 4\ell$  is illustrated in the left panel of Fig. 1. The four  $Z$  decay momenta coming from a heavy Higgs-like state  $X$  are given by

$$p_X = p_{Z_e} + p_{Z_\mu}, \quad p_{Z_e} = p_{e^-} + p_{e^+}, \quad p_{Z_\mu} = p_{\mu^-} + p_{\mu^+}. \quad (1)$$

For each of these momenta and the beam direction we define unit three-momenta  $\hat{p}_i$  in the  $X$  rest frame and in the two  $Z_{e,\mu}$  rest frames. Note that the one of the two  $Z$  bosons will be far of its mass shell, i.e.  $p^2 \ll m_Z^2$ , but this does not pose a problem for the boost into its reference frame. The set of observable spin and CP angles are then defined

$$\begin{aligned} \cos \theta_e &= \hat{p}_{e^-} \cdot \hat{p}_{Z_\mu} \Big|_{Z_e} & \cos \theta_\mu &= \hat{p}_{\mu^-} \cdot \hat{p}_{Z_e} \Big|_{Z_\mu} & \cos \theta^* &= \hat{p}_{Z_e} \cdot \hat{p}_{\text{beam}} \Big|_X \\ \cos \phi_e &= (\hat{p}_{\text{beam}} \times \hat{p}_{Z_\mu}) \cdot (\hat{p}_{Z_\mu} \times \hat{p}_{e^-}) \Big|_{Z_e} & \cos \Delta\phi &= (\hat{p}_{e^-} \times \hat{p}_{e^+}) \cdot (\hat{p}_{\mu^-} \times \hat{p}_{\mu^+}) \Big|_X. \end{aligned} \quad (2)$$

The index at the end of each relation indicates the rest frame in which the angles are defined. In the notation in Ref. [15] this corresponds to  $\phi_e \rightarrow \Phi_1$  and  $\Delta\phi \rightarrow \Phi$ . An important feature is that the reconstruction of the angles defined in Eq.(2) requires a full reconstruction of the ‘Higgs’ decay at all stages. It does not require both  $Z$  bosons to be on-shell as long as we can boost into a well-defined center-of-mass frame of the two decay leptons. In spite of the suggestive notation the angles  $\phi$  and  $\theta$  do not stand for opening angles and not azimuthal or polar angles.

As a first illustration we show the  $\Delta\phi$  dependences for the process  $pp \rightarrow X \rightarrow ZZ \rightarrow (e^+e^-)(\mu^+\mu^-)$  in the left panel of Fig. 2. Our hypotheses are the three allowed scalar  $XZZ$  couplings structures to mass dimension six (or five after symmetry breaking) [11, 27] and a spin-2 operator [12]. The corresponding operators are spelled out in Sec. III A and III C.

For the Standard Model coupling we expect this distribution to have a mild modulation, which would vanish for large Higgs masses. In contrast, there are clear modulations in  $\Delta\phi$  with a phase shift between CP-even and CP-odd dimension-5 operators, which can be easily understood from kinematics [11, 12].

The  $X \rightarrow ZZ \rightarrow 4\ell$  topology and the weak-boson-fusion ‘Higgs’ production topology

$$q_1 q_2 \rightarrow j_1 j_2 (X \rightarrow d\bar{d}) \quad (3)$$

are linked by a crossing symmetry. The labeling of the incoming and outgoing partons as incoming quarks  $q_{1,2}$  and outgoing jets  $j_{1,2}$  is only meant to allow for a definition of the angles independently of the partonic sub-processes. The ‘Higgs’ decay products can be  $d = \tau, W, Z, \gamma$ , depending on the channel we are looking at [28–30]. For those observables which require a full momentum reconstruction of  $p_d$  the list of useful Higgs decay channels is reduced.

Our aim is to generalize the angular basis of Eq.(2) to weak boson fusion, guided by the obvious crossing symmetry. When moving one of the final state partons to the initial state we replace time-like  $Z$  propagators with space-like  $V = W, Z$  propagators in the  $t$ -channel. In this situation we know that the corresponding Breit

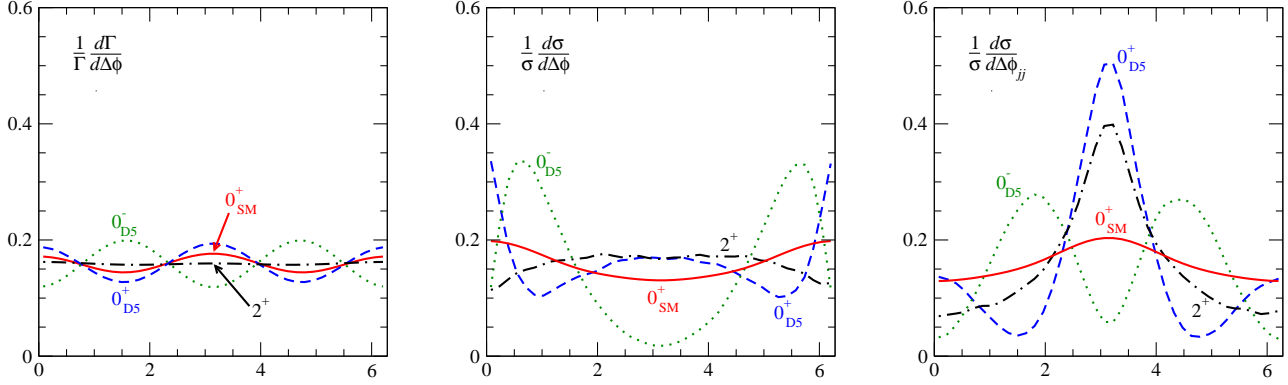


Figure 2: Normalized  $\Delta\phi$  distributions for  $X \rightarrow ZZ$  events (left), WBF production in the Breit frame (center), and WBF production in the laboratory frame (right). We show the SM operator  $XV_\mu V^\mu$  (solid), the CP-even dimension-5 operator  $XV_{\mu\nu}V^{\mu\nu}$  (dashed), the CP-odd dimension-5 operator  $XV_{\mu\nu}\tilde{V}^{\mu\nu}$  (dotted), and an example for a spin-2 coupling (dashed-dotted). The operators are defined in Secs. III A and III C.

frames are the appropriate reference frames. It is defined as the reference frame where the momentum of the  $t$ -channel particle  $V$  is completely space-like and can be reached through a conventional boost. Similar to the  $X \rightarrow ZZ$  case, a full reconstruction of the  $X$  decay is required. With this caveat and fixing the directions of all the external momenta as shown in Fig. 1 we define a modified version of the five angles in Eq.(2),

$$\begin{aligned} \cos\theta_1 &= \hat{p}_{j_1} \cdot \hat{p}_{V_2} \Big|_{V_1 \text{ Breit}} & \cos\theta_2 &= \hat{p}_{j_2} \cdot \hat{p}_{V_1} \Big|_{V_2 \text{ Breit}} & \cos\theta^* &= \hat{p}_{V_1} \cdot \hat{p}_d \Big|_X \\ \cos\phi_1 &= (\hat{p}_{V_2} \times \hat{p}_d) \cdot (\hat{p}_{V_2} \times \hat{p}_{j_1}) \Big|_{V_1 \text{ Breit}} & \cos\Delta\phi &= (\hat{p}_{q_1} \times \hat{p}_{j_1}) \cdot (\hat{p}_{q_2} \times \hat{p}_{j_2}) \Big|_X. \end{aligned} \quad (4)$$

Again, we define the angle between the two planes of the Breit frames as  $\Delta\phi$ . We will see below that this angle is similar to the azimuthal difference of two jets in the laboratory frame,  $\Delta\phi_{jj}$ , even though in Eq.(4)  $\phi$  and  $\theta$  do not imply azimuthal or polar angles. It should be noted that using these conventions we can define the angle  $\Phi_+ \equiv 2\phi_1 + \Delta\phi$  which typically lead to modulations for spin-2 resonances. In the notation of the Ref. [12] this corresponds to  $\Phi_+ \rightarrow \Phi_{12}$ .

Since we cannot measure the charge of the four fermions involved in the WBF topology, we need an alternative criterion to map the leptonic observables in Eq.(2) to an LHC production process. We break the external fermion degeneracy by imposing that each incoming quark  $q_{1,2}$  largely keeps its direction when the scattering process turns into a tagging jet  $j_{1,2}$ . This defines the weak boson 3-momenta

$$\vec{p}_{V_{1,2}} = \vec{p}_{q_{1,2}} - \vec{p}_{j_{1,2}}, \quad (5)$$

where  $q_{1,2}$  are the incoming partons moving in the beam direction,  $\hat{p}_{q_{1,2}} = \pm \hat{e}_{\text{beam}}$ .

Technically, the determination of the incoming particle momenta  $q_{1,2}$  is an issue at hadron colliders (and ill-defined in perturbative QCD). We start by reconstructing the final state and map it onto a set of partonic momenta. In the absence of additional jet radiation this defines the center-of-mass system for the incoming quarks, related to the laboratory frame by a longitudinal boost. The incoming parton momenta are parameterized as  $p_{q_1} = (E_1, 0, 0, E_1)$  and  $p_{q_2} = (E_2, 0, 0, -E_2)$ , which we can invert to express  $E_1$  and  $E_2$  in terms of the summed energy and longitudinal momentum entries of the final state particles. The boost from the laboratory frame to the center-of-mass system can be approximated by reconstructing the events' pseudorapidity from the detector geometry and massless calorimeter hits. This should be understood as a prescription to obtain a set of well-defined (leading order, parton-like) four-momenta rather than reconstructing the actual initial state.

Among the angles listed in Eq.(4)  $\Delta\phi$  does not require a reconstruction of the Higgs candidate. It is constructed only from the four external partons, two incoming and two outgoing. Comparing Eq.(4) and Eq.(2) we see that it corresponds to the angle between the two  $Z$  decay planes in  $X \rightarrow ZZ$  decays. In the central panel of Fig. 2 we show it for illustration, testing the same three spin-0 hypotheses as in the left panel and properly defined in Sec. III A. The Standard Model expectation is again relatively flat, with an additional residual dependence introduced the interference of longitudinal and transverse amplitudes and by kinematic cuts. The two dimension-5 operators show a distinct modulation, in complete analogy to the corresponding measurement in  $X \rightarrow ZZ$  decays, but with a larger amplitude of the modulation.

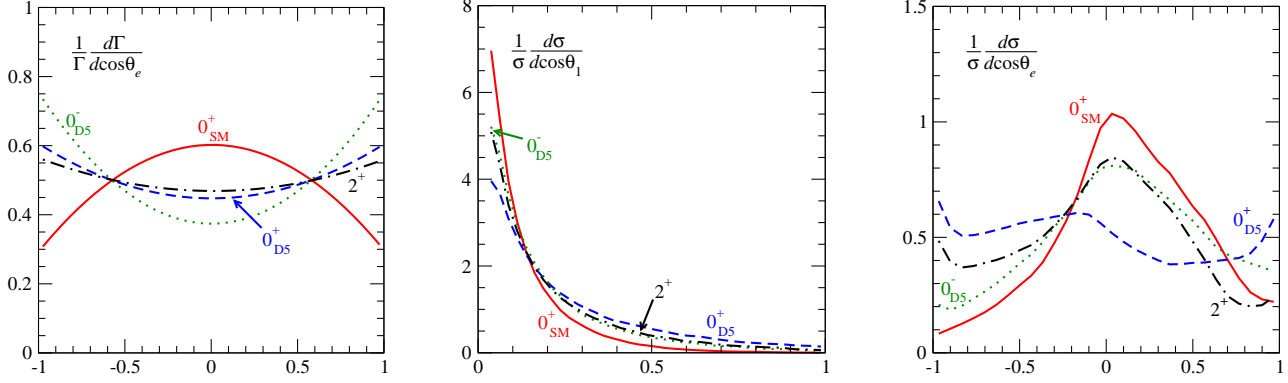


Figure 3: Normalized  $\cos\theta$  distributions for  $X \rightarrow ZZ$  events (left), WBF production in the Breit frame (center), and WBF production after analytic continuation (right). Again, we show  $XV_\mu V^\mu$  (solid),  $XV_{\mu\nu} V^{\mu\nu}$  (dashed),  $XV_{\mu\nu} \tilde{V}^{\mu\nu}$  (dotted), and the spin-2 example (dashed-dotted), as defined in Secs. III A and III C.

A second key observable in the angular analysis of the  $X \rightarrow ZZ$  topology is the helicity angle  $\theta_{e,\mu}$ . In the left panel of Fig. 3 we show how it discriminates between a spin-0 and spin-2 resonance [15]. The spin-2 Lagrangian is defined in Sec. III C. For the crossed WBF topology the center panel shows the Breit frame version, defined in Eq.(4). It is only of limited use to differentiate between the different hypotheses.

The translation of the  $H \rightarrow ZZ$  angles into the Breit frame basis of Eq.(4) is not the only possible generalization. To avoid a boost into the Breit frame we can alternatively construct a crossed set of momenta simply mapping the  $pp \rightarrow Xjj$  kinematics to the  $X \rightarrow 4\ell$  kinematics. This way we can show the distributions in terms of the angles defined in Eq.(2): the WBF topology is related to the decay  $X \rightarrow ZZ \rightarrow 4\ell$  via the crossing symmetry  $p_{q_i} \rightarrow -p_{q_i}$ . This crossing we can perform by analytically continuing the WBF initial state momenta to final state momenta, rendering  $p_V$  time-like. We illustrate this alternative mapping to space-like momenta  $p_V$  in the right panel of Fig. 3, including basic acceptance cuts. We see that this observable is more distinctive than its Breit frame counterpart, but not as clear as the decay angle correlation.

The different observations discussed in this section gives us confidence that a detailed study of angular correlation in WBF events should serve as a powerful supplement to the study of  $X \rightarrow ZZ$  decays.

Additional observables have been suggested for a dedicated study of a spin-2 resonance. One of them is the sum of the two  $V_{1,2}$  Breit frame angles  $\Phi_+$  [12]. Another is the so-called Gottfried–Jackson angle  $\theta_{GJ}$  [31, 32]. It is the angle between the momentum of the resonance  $X$  in the laboratory frame and one of the  $X$  decay products in the  $X$  rest frame (somewhat in analogy of the top helicity angle). Compared to the angular basis of Eq.(4) it is very closely related to  $\theta^*$ , as confirmed in Fig. 4. For spin-0 and spin-1 both distributions show a flat behavior, as shown in the Appendix. For spin-2 the two angles are essentially equivalent. It will turn out that the angle  $\theta^*$  appears to be more stable with respect to UV completions or the presence of form factors appearing in the spin-2 theory, so we will focus on  $\theta^*$  in the following.

## B. Hadron collider observables

While the kinematic observables introduced in Eq.(4) are well suited to capture the properties of a Higgs candidate and its coupling to gauge bosons, they are not particularly well suited to cope with QCD effects at hadron colliders. The reason is that the reconstruction of the  $V_{1,2}$  Breit frames assumes a complete reconstruction of the hard scattering process. This assumption is not realistic in the presence of QCD jet radiation on the one hand and underlying event and pile-up on the other hand.

As a rough guide line we can look at the opening angle between the two  $Z$  decay planes in  $X \rightarrow ZZ$  decays again. For the WBF production process it turns into  $\cos\Delta\phi = (\hat{p}_{q_1} \times \hat{p}_{j_1}) \cdot (\hat{p}_{q_2} \times \hat{p}_{j_2})$ , evaluated in the Higgs candidate’s rest frame. In the laboratory frame each vector  $(\hat{p}_q \times \hat{p}_j)$  by definition resides in the azimuthal plane. In the Higgs candidate’s rest frame this changes, but the impact of a modest transverse boost on the large longitudinal parton momenta should be small as well. If we compute  $\Delta\phi$  in the laboratory frame instead, it turns into the azimuthal angle between two vectors, each orthogonal to one of the tagging jet direction. This is equivalent to the azimuthal angle between the two tagging jets  $\Delta\phi_{jj}$ . In the right panel of Fig. 2 we show this azimuthal opening angle for the WBF production of four Higgs candidates, with the scalar tree-level

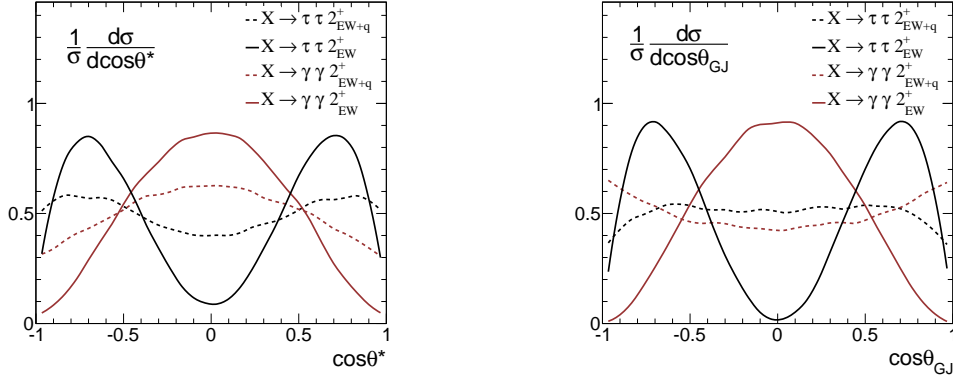


Figure 4: Normalized  $\cos \theta^*$  and  $\cos \theta_{GJ}$  distributions for a spin-2 resonance coupling only to weak bosons or coupling to quarks as well. We show the  $X$  decay to tau leptons and to photons.

and dimension-5  $XVV$  couplings or a spin-2 coupling. As expected, the Standard Model operator predicts an essentially flat behavior, while the other two show a distinctly different modulation [11, 21], arguably the strongest of the three approaches compared in this figure.

Encouraged by this observation we define a new set of (essentially) angular correlations for the WBF Higgs production process

$$q_1 q_2 \rightarrow j_1 j_2 (X \rightarrow d\bar{d}) . \quad (6)$$

It simply uses the rapidity differences and azimuthal opening angles between the tagging jets, the Higgs candidate (if reconstructed), and its decay products:

$$\{\Delta\eta_{mn}, \Delta\phi_{mn}\} \quad \text{for } m, n = j_{1,2}, X, d, \bar{d} . \quad (7)$$

The two tagging jets  $j_{1,2}$  now have to be ordered, so we defined  $j_1$  to be harder of the two. Should there be additional jets in the event we choose the hardest two jets which qualify as tagging jets following the basic cuts defined in Sec. IV.

Obviously, this set of observables over-constrains the kinematics in the laboratory frame. The dimensionality of the phase space is eight, which includes only five independent angles. While the collider observables of Eq.(7) might not be the most obvious choice for testing spin and CP properties of a heavy resonance  $X$ , the case of  $\Delta\phi_{jj}$  shows their potential, and they are well-defined experimental quantities at hadron colliders.

One additional observable of interest is the boost which relates the lab frame to the ‘Higgs’ and the partonic  $Xjj$  center-of-mass frames. It is related to the kind of parton in the initial state, distinguishing valence quarks from sea quarks or gluons. While it is possible to for example construct asymmetries in the two frames, we do not find clear links to the coupling structure of a massive particle in weak boson fusion.

Finally, at least for a cross check it might be useful to add information which is not encoded in the rapidity differences or angles in Eq.(7). One such observable is the transverse momentum of the tagging jet, where the splitting probability  $P_{T,L}(x)$  is known to look different for transverse and longitudinally polarized gauge bosons [10, 33]

$$\begin{aligned} P_T(x, p_T) &\propto \frac{1 + (1-x)^2}{2x} \frac{p_T^2}{(p_T^2 + (1-x)m_W^2)^2} \rightarrow \frac{1 + (1-x)^2}{2x} \frac{1}{p_T^2} \\ P_L(x, p_T) &\propto \frac{1-x}{x} \frac{m_W^2}{(p_T^2 + (1-x)m_W^2)^2} \rightarrow \frac{1-x}{x} \frac{m_W^2}{p_T^4} . \end{aligned} \quad (8)$$

Looking at large transverse momenta  $p_T \gg m_V$  the radiation of longitudinal  $V$  bosons falls off sharper than the radiation of transverse  $V$  bosons. Even more distinctively, for spin-1 or spin-2 particle production we know that these states do not unitarize the partonic processes. This difference can have a huge effect on the transverse momenta of the tagging jets [34, 35], depending on the additional unitarization procedure.

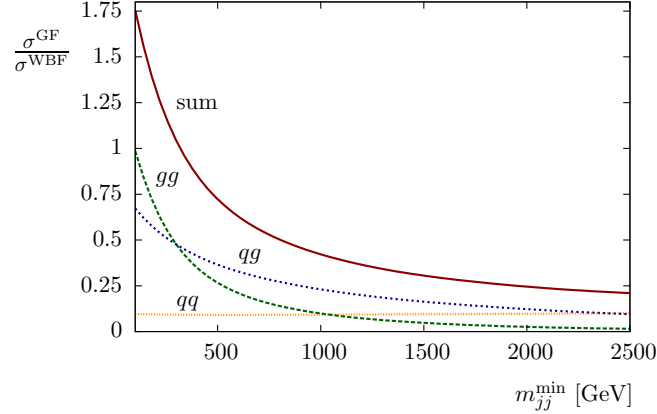


Figure 5: Contamination of WBF Higgs events with gluon-fusion events as a function of  $m_{jj}^{\text{min}}$ . Note that the unphysical separation of the partonic processes contributing to the order  $\alpha_s^2 g_{Hgg}^2$  is only possible at leading order and scale dependent. The NLO rates are based on VBFNLO [20, 36].

### C. Contaminating sub-processes

The main advantage of the leptonic decay  $H \rightarrow ZZ \rightarrow 4\ell$  is that after some basic kinematic cuts the backgrounds are negligible. This holds for non-Higgs events, for example from continuum  $ZZ$  production, but also for signal events which might have different topology or different intermediate states.\*

Once we switch to WBF Higgs production the non-Higgs backgrounds are still small,  $S/B = \mathcal{O}(1)$ , but not entirely negligible. The angular correlations for example of the  $Z \rightarrow \tau\tau$  background process is well understood, which means that they can be taken into account in the final analysis [11]. Additional partonic sub-process contributing to WBF Higgs production are

$$q\bar{q} \rightarrow q\bar{q}H, ggH \quad qg \rightarrow qgH \quad \bar{q}q \rightarrow \bar{q}qH \quad gg \rightarrow q\bar{q}H, ggH, \quad (9)$$

all mediated by the effective  $Hgg$  coupling, i.e. with cross sections of the order  $\sigma \propto \alpha_s^2 g_{Hgg}^2$ . *Per se*, these rates are not small. After the basic acceptance cuts, shown in Sec. IV, they can exceed the WBF signal. However, to remove the QCD-induced  $Zjj$  background at order  $\alpha\alpha_s^2$  we need to apply a stiff cut on the invariant mass of the two tagging jets  $m_{jj} > 600 - 800$  GeV. This cut reduces the contamination of gluon-fusion Higgs events in the WBF sample to a small perturbation.

In Fig. 5 we show the relative size of the Higgs production rates in gluon fusion and in weak boson fusion. Indeed, for  $m_{jj}^{\text{min}} \sim 250$  the two production modes still contribute with similar rates. When we increase  $m_{jj}^{\text{min}}$  towards 1 TeV the combined gluon fusion contribution rapidly falls off. Splitting it into the different contributions of order  $\alpha_s^2 g_{Hgg}^2$ , as given by the partonic sub-processes, we see that the originally dominant  $gg$  initial state drops below 20% of the WBF rate around  $m_{jj}^{\text{min}} \sim 500$  GeV. The mixed quark-gluon initial state is the most dangerous, because it is almost as large as the gluon fusion rate, but it drops only very slowly with a remaining 30% correction to the weak boson fusion rate for realistic  $m_{jj}^{\text{min}}$  values. In contrast, the purely quark-induced sub-process gives a constant correction around 10% and cannot be reduced choosing larger  $m_{jj}^{\text{min}}$  values.

In combination, after applying tagging jet acceptance cuts and the usual  $m_{jj}^{\text{min}}$  cut we roughly expect one third of the Higgs signal events to arise from gluon fusion. However, in a realistic analysis we need a minijet veto to further reduce the  $t\bar{t}$  and QCD  $Z$ +jets backgrounds. The original (still largely valid) estimates for the survival probabilities against such a veto range around 90% for the WBF signal and 30% for the QCD  $Z$ +jets background [28, 29]. Gluon fusion Higgs production will be even more strongly suppressed, with a recently estimated jet veto survival probability below 20% [37, 38]. This means that after applying such a jet veto the gluon fusion contamination will drop from 50% to a negligible 10%. For  $m_{jj} > 1$  TeV it ranges around 3%. The

\* A potentially dangerous contribution would be from Higgs decays to  $Z\gamma$ , where for a dimension-5  $HZZ$  coupling we would not expect any hierarchy between the effective  $g_{HZZ}$  and  $g_{HZ\gamma}$  couplings.



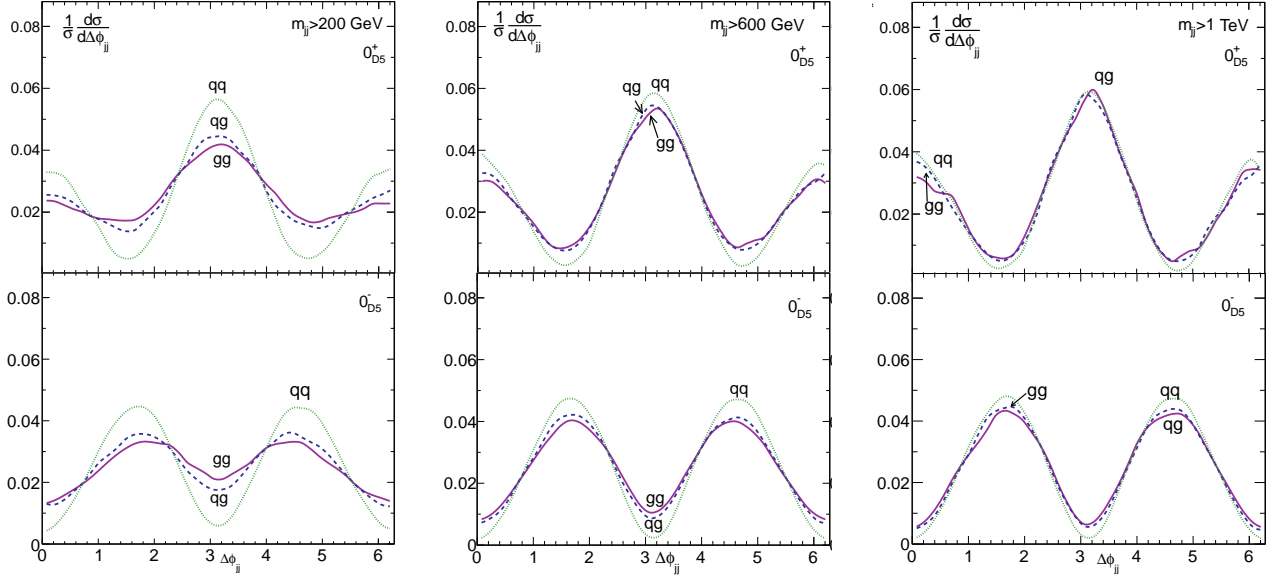


Figure 6: Normalized  $\Delta\phi_{jj}$  distributions for Higgs production in gluon fusion, separated by partonic channels to leading order. The CP even Higgs is represented on the top figures and the CP odd on the bottom ones. The  $m_{jj}^{\min}$  cut is increased from 200 GeV (left) to 600 GeV (central) and 1 TeV (right).

interference between gluon fusion and WBF diagrams can be safely neglected, essentially independently of the cuts [39]. In our detailed analysis we therefore omit all gluon-induced operators and show the corresponding distributions only in the Appendix.

In addition to the fact that the WBF Higgs event sample will only have a small contribution from gluon fusion, there is no problem in carrying a percentage of gluon fusion event through the Higgs coupling analysis. For example, for a scalar Higgs boson the CP quantum number entirely fixes the form of the effective  $Hgg$  coupling structure. As an example, in Fig. 6 we show the  $\Delta\phi_{jj}$  distribution for gluon fusion Higgs production, split into the three partonic sub-processes listed in Eq.(9). The partonic sub-processes show a very similar behavior, essentially independent of the detailed cuts. Once we require at least  $m_{jj}^{\min} = 600$  GeV the curves are completely degenerate. The effective Higgs-gluon coupling in the Standard Model has the same structure as the CP-even dimension-5 operator for weak gauge bosons,  $HV_{\mu\nu}V^{\mu\nu}$ , which explains the quantitative agreement of these results with the right panel of Fig 2. The  $m_{jj}^{\min}$  cut forces all partonic sub-channels into similar kinematic configurations, while the Higgs production is governed by the same coupling to mostly  $t$ -channel gluons. If there should be a good reason to include more gluon-fusion Higgs events in this coupling analysis we can expect stable results in the combination of gluon fusion and weak boson fusion, without any complications from different partonic sub-processes governed by the parton densities.

Finally, an additional complication in WBF is the fact that we cannot determine the charge of the incoming and outgoing fermions, *i.e.* we cannot distinguish neutral from charged current contributions. As long as we stick to  $SU(2)$ -invariant operators this does not pose a problem, but there exist Higgs-candidate operators which are forbidden by the Bose symmetry between two  $Z$  bosons and allowed for a  $W^+W^-$  pair. In Sec. IIIB we will come across them. While we can distinguish photon-induced contributions based on the transverse momentum spectrum of the tagging jets,  $WW$  and  $ZZ$  induced WBF events are indistinguishable, with a typical relative size 1 : 4, dominated by  $WW$  fusion.

### III. LAGRANGIAN

Measuring the Higgs coupling structure in weak boson fusion is not a theory-independent measurement. Instead, we have to implement all different hypotheses in a Monte Carlo event generator, *i.e.* MADGRAPH [40]. The different predictions then have to be compared to ATLAS and CMS data. In Section IV we will limit ourselves to signal-only results, noting that in WBF Higgs searches we expect a favorable signal-to-background ratio. Moreover, we will only show a limited number of particularly promising distributions to show that we can



indeed distinguish all available scenarios for a heavy resonance  $X$ . A complete list of all simulated distributions can be found in the Appendix.

### A. Spin zero

The different hypotheses for the nature of a heavy resonance  $X$  can be easily ordered by its spin. First, we parameterize the relevant interactions of a CP-even or CP-odd scalar  $X = H, A$  with gauge bosons in an effective, gauge-invariant Lagrangian [11, 27, 41],

$$\mathcal{L}_0 = g_1^{(0)} H V_\mu V^\mu - \frac{g_2^{(0)}}{4} H V_{\mu\nu} V^{\mu\nu} - \frac{g_3^{(0)}}{4} A V_{\mu\nu} \tilde{V}^{\mu\nu} - \frac{g_4^{(0)}}{4} H G_{\mu\nu} G^{\mu\nu} - \frac{g_5^{(0)}}{4} A G_{\mu\nu} \tilde{G}^{\mu\nu}, \quad (10)$$

where  $V = W, Z$  are the electroweak gauge bosons and  $G$  is the gluon. The coupling to the photon can be described in complete analogy, but it will not be relevant for our analysis of LHC production channels. For all gauge fields the corresponding  $V^{\mu\nu}$  indicates the field strength tensor and  $\tilde{V}^{\mu\nu}$  is its dual. Some of the couplings  $g_i^{(0)}$  defined this way have mass dimension, i.e. we do not distinguish between order-one coupling factors and mass suppression. This simplified notation is appropriate, since throughout our analysis we assume equal rates for all coupling operators. In the Standard Model the couplings are  $g_1^{(0)} = 2M_V^2/v$  and  $g_4^{(0)} = \alpha_s g_{Htt}/3\pi v$  (in the heavy top limit) [10]. The additional higher-dimensional coupling  $g_2^{(0)}$  is finite but negligible in the Standard Model.

In an effective theory approach the couplings  $g_2^{(0)} - g_5^{(0)}$ , which carry mass dimension  $1/\Lambda$ , can be generated through loops. We omit the additional factors  $1/\Lambda$  throughout our discussion because it complicates the notation and will be of no relevance to our discussion of angular correlations. Nevertheless, we expect a hierarchy in the size of scalar ‘Higgs’ couplings. In general, the far off-shell processes  $H \rightarrow ZZ \rightarrow 4\ell$  and  $H \rightarrow WW \rightarrow \ell^+ \ell^- \nu \bar{\nu}$  come with an additional suppression factor from the leptonic branching ratios. In contrast, there is no such suppression for the loop-induced decay  $H \rightarrow \gamma\gamma$ . In absence of the Standard Model coupling  $g_1^{(0)}$  the LHC measurements require  $g_2^{(0,ZZ)} \approx g_2^{(0,WW)} \approx 1000 g_2^{(0,\gamma\gamma)}$ . The non-diagonal coupling  $g_2^{(0,Z\gamma)}$  is similarly suppressed in the absence of an on-shell  $H \rightarrow Z\gamma$  signal. However, as long as anomaly-free  $SU(2)$  multiplets run inside the loops all induced couplings tend to be of similar size. This implies that a substantial fine tuning would be needed to accommodate a  $g_2^{(0)}$ -based explanation of the ATLAS and CMS results.

While such an argument based on relative rates is convincing in an effective theory framework with an essentially known particle content, the analysis of angular correlations is model independent. It does not assume any perturbative field theory and hence applies to all possible fundamental explanations of the ‘Higgs’ sector of the Standard Model. The list of scalar hypotheses which we test later is summarized in Tab. I.

### B. Spin one

The general Lagrangian describing the interaction between a neutral CP-even or CP-odd gauge boson  $X = Y^{(e)}, Y^{(o)}$  and the electroweak gauge bosons is

$$\begin{aligned} \mathcal{L}_1 = & ig_1^{(1)} (W_{\mu\nu}^+ W^{-\mu} - W_{\mu\nu}^- W^{+\mu}) Y^{(e)\nu} + ig_2^{(1)} W_{\mu\nu}^+ W_{\nu}^- Y^{(e)\mu\nu} \\ & + g_3^{(1)} \epsilon^{\mu\nu\rho\sigma} (W_{\mu}^+ \overleftrightarrow{\partial}_{\rho} W_{\nu}^-) Y_{\sigma}^{(e)} + ig_4^{(1)} W_{\sigma\mu}^+ W^{-\mu\nu} Y_{\nu}^{(e)\sigma} \\ & - g_5^{(1)} W_{\mu}^+ W_{\nu}^- (\partial^{\mu} Y^{(o)\nu} + \partial^{\nu} Y^{(o)\mu}) + ig_6^{(1)} W_{\mu}^+ W_{\nu}^- \tilde{Y}^{(o)\mu\nu} + ig_7^{(1)} W_{\sigma\mu}^+ W^{-\mu\nu} \tilde{Y}_{\nu}^{(o)\sigma} \\ & + g_8^{(1)} \epsilon^{\mu\nu\rho\sigma} Y_{\mu}^{(e)} Z_{\nu} (\partial_{\rho} Z_{\sigma}) + g_9^{(1)} Y_{\mu}^{(o)} (\partial_{\nu} Z^{\mu}) Z^{\nu}. \end{aligned} \quad (11)$$

It includes  $g_1^{(1)} - g_7^{(1)}$  describing the coupling to  $W$  bosons [27] and the reduced set  $g_8^{(1)} - g_9^{(1)}$  for the  $Z$  couplings [42], constrained by the Landau-Yang theorem [26]. All terms in this Lagrangian have mass dimension four, except for  $g_4^{(1)}$  and  $g_7^{(1)}$ . Compared to the usual  $X \rightarrow ZZ$  analysis this WBF Lagrangian is much more complex, so we limit our number of hypotheses to one coupling each for CP-even and CP-odd states to  $W$  and  $Z$  bosons,

$$\begin{aligned} 1_W^+ : & \quad g_1^{(1)} = g_2^{(1)} \neq 0 & 1_W^- : & \quad g_5^{(1)} = g_6^{(1)} \neq 0 \\ 1_Z^+ : & \quad g_8^{(1)} \neq 0 & 1_Z^- : & \quad g_9^{(1)} \neq 0 \end{aligned} \quad (12)$$

	initial state	couplings	
$0_{\text{SM}}^+$	$qq$	$g_1^{(0)}$	SM Higgs scalar (D3 coupling to $W, Z$ )
$0_{\text{D5}}^+$	$qq$	$g_2^{(0)}$	scalar (D5 coupling to $W, Z$ )
$0_{\text{D5}}^-$	$qq$	$g_3^{(0)}$	pseudo-scalar (D5 coupling to $W, Z$ )
$0_{\text{D5g}}^+$	$qq, qg, gg$	$g_4^{(0)}$	scalar (D5 coupling to gluons)
$0_{\text{D5g}}^-$	$qq, qg, gg$	$g_5^{(0)}$	pseudo-scalar (D5 coupling to gluons)
$1_W^-$	$qq$	$g_5^{(1)} = g_6^{(1)}$	D4 couplings to $W$
$1_Z^-$	$qq$	$g_9^{(1)}$	vector coupling to $Z$
$1_W^+$	$qq$	$g_1^{(1)} = g_2^{(1)}$	D4 couplings to $W$
$1_Z^+$	$qq$	$g_8^{(1)}$	axial-vector coupling to $Z$
$2_{\text{EW}}^+$	$qq$	$g_1^{(2)}$	tensor coupling to EW gauge bosons
$2_{\text{EW+q}}^+$	$qq, qg, gg$	$g_1^{(2)} = g_3^{(2)}$	tensor coupling to EW gauge bosons and fermions
$2_{\text{QCD}}^+$	$qq, qg, gg$	$g_2^{(2)}$	tensor coupling to gluons
$2^+$	$qq, qg, gg$	$g_1^{(2)} = g_2^{(2)} = g_3^{(2)}$	graviton-like tensor

Table I: Properties of the heavy resonance models discussed in this paper. The structure of the coupling to gluons we only list for completeness reasons, in the analysis we do not have to take these operators into account. Instead, we show them in the Appendix.

The interactions of  $Y^{(e)}$  with  $W$  bosons has the same form as for a Kaluza-Klein  $Z$  boson, *i.e.* it is a re-scaled version of the  $WWZ$  coupling in the Standard Model. For the CP-odd  $Y^{(o)}$  we resort to a special combination of dimension-4 operators only. The interactions with  $Z$  bosons is the usual complete basis [14–16]. These four scenarios are summarized in Tab. I. We will see that the angular correlations in WBF production of a  $1_W^\pm$  and  $1_Z^\pm$  can be different. The reason is that in our choice of operators the two are at best partially identical, because the list of allowed coupling structures of a neutral resonance to the neutral  $Z$  is considerably more constrained.

When extending our analysis of the WBF production process to include decays of the heavy neutral resonance for example into a pair of  $\tau$  leptons we need to assume a structure of its coupling to fermions. For simplicity, we assume the same vector and axial-vector structure as the  $Z$  boson,

$$g_V = -\frac{1}{2} + 2\sin^2\theta_w \quad g_A = -\frac{1}{2}, \quad (13)$$

again re-scaled by a constant factor. Moreover, we only couple the new vector to the third generation, to avoid modifications of the WBF production process.

### C. Spin two

There is a number of commonly used ways to parameterize the interaction of a spin-2 boson [15]. As usually, we choose graviton-inspired scenarios to contrast with the scalar Higgs boson. More precisely, we consider a massive graviton resonance, which couples to the SM particles through their energy-momentum tensors,

$$\mathcal{L}_2 = -g_1^{(2)} G_{\mu\nu} T_V^{\mu\nu} - g_2^{(2)} G_{\mu\nu} T_G^{\mu\nu} - g_3^{(2)} G_{\mu\nu} T_f^{\mu\nu}, \quad (14)$$

where  $G_{\mu\nu}$  is the spin-2 resonance and  $T_{V,G,f}^{\mu\nu}$  is the energy-momentum tensor of the electroweak gauge bosons, the gluon, and the different fermions. For instance, the tensor for the  $Z$  boson is given by [43]

$$T_Z^{\mu\nu} = -g^{\mu\nu} \left[ -\frac{1}{4} Z_{\rho\sigma} Z^{\rho\sigma} + \frac{m_Z^2}{2} Z_\rho Z^\rho \right] - Z_\rho^\mu Z^{\nu\rho} + m_Z^2 Z^\mu Z^\nu$$

with  $Z_{\mu\nu} = \partial_\mu Z_\nu - \partial_\nu Z_\mu + ig_w \cos\theta_w (W_\mu^+ W_\nu^- - W_\nu^+ W_\mu^-)$ .

(15)

While conventional graviton excitations have universal couplings strengths  $1/\Lambda$  to fermions and gauge fields, where  $\Lambda$  is the scale parameter of the theory, for our test we define four scenarios motivated on the WBF

topology

$$\begin{aligned}
2_{\text{EW}}^+ : \quad & g_1^{(2)} = \frac{1}{\Lambda} \quad g_2^{(2)} = g_3^{(2)} = 0 , \\
2_{\text{EW}+q}^+ : \quad & g_1^{(2)} = g_3^{(2)} = \frac{1}{\Lambda} \quad g_2^{(2)} = 0 , \\
2_{\text{QCD}}^+ : \quad & g_2^{(2)} = \frac{1}{\Lambda} \quad g_1^{(2)} = g_3^{(2)} = 0 , \\
2^+ : \quad & g_1^{(2)} = g_2^{(2)} = g_3^{(2)} = \frac{1}{\Lambda} .
\end{aligned} \tag{16}$$

A universally-coupled spin-2 particle is heavily constrained by Tevatron data [44], but we ignore these constraints in our discussion limited to the Higgs sector. All hypotheses shown in Tab. I are not meant as a valid ultraviolet completion of the Standard Model without a Higgs boson. All they need to serve as are general alternative scenarios for the interpretation of a Higgs-like resonance in weak boson fusion. Similar to the spin-1 case, the couplings to leptons are assumed to include decays of the spin-2 resonance even for  $2_{\text{EW}}^+$  and  $2_{\text{QCD}}^+$ .

#### IV. ANALYSIS

The study presented in this section is not meant to produce an optimized Higgs couplings analysis using the weak-boson-fusion production mechanism. Instead, we study the behavior of the kinematic variables described in Sec. II B for the different ‘Higgs’ candidates. For this purpose, we identify the most promising variables to separate the different Higgs spins and couplings defined in Secs. III A-III C. Based on this most promising subset of observables we will show how the different hypotheses on the nature and the couplings of the heavy state  $X$  can be distinguished. In Sec. IV E we apply a more sophisticated statistical analysis to this problem, but eventually we will leave it to the LHC experiments to determine the quantitative impact of our approach.

For our numerical analysis we implement the interactions Lagrangians Eqs.(10), (11) and (14) into FEYN-RULES [45], which provides a UFO model file [46] that we implement into MADGRAPH5 [40]. All simulations for this section are done at parton level for an LHC energy of 14 TeV. To study the impact of the acceptance cuts on our observables we choose three possible set of acceptance cuts:

1. We start with a minimal set of cuts applied on the outgoing partons

$$p_{T,j} \geq 20 \text{ GeV} \quad \Delta R_{jj} \geq 0.6 \quad |\eta_j| \leq 5 . \tag{17}$$

2. To suppress backgrounds and a possible contamination with gluon-fusion events we also include

$$m_{jj} \geq 600 \text{ GeV} . \tag{18}$$

3. As is common in WBF analyses we require a rapidity gap between the two tagging jets

$$\Delta\eta_{jj} \geq 4.2 \quad \eta_{j_1} \times \eta_{j_2} < 0 . \tag{19}$$

Note that while we simulate the decay  $X \rightarrow \tau\tau$  [11, 28] as a toy channel for including the  $X$  momentum and the momentum of the decay product we do not apply any cuts on the decay products. In Tab. II we present the signal and background ratio suppression after cutting on  $m_{jj}$ , Eq.(18), and after requiring the rapidity gap between the two tagging jets, Eq.(19). The signal and the backgrounds are normalized to the rates after the acceptance cuts of Eq.(17). We see that the background suppression and the reduced contamination from gluon-fusion are delivered by the  $m_{jj}$  cut. In the following we will advocate that the cuts from Eq.(19) should

cuts	signal										background $\tau\tau jj$	
	$0_{\text{SM}}^+$	$0_{\text{D5}}^+$	$0_{\text{D5}}^-$	$0_{\text{D5g}}^+$	$0_{\text{D5g}}^-$	$1_W^+$	$1_W^-$	$1_Z^+$	$1_Z^-$	$2^+$	EW	QCD
$m_{jj}$ in Eq.(18)	0.442	0.241	0.290	0.072	0.070	0.318	0.420	0.291	0.419	0.161	0.211	0.027
$\Delta\eta_{jj}$ in Eq.(19)	0.389	0.068	0.108	0.053	0.053	0.189	0.242	0.134	0.220	0.096	0.124	0.014

Table II: Signal and background cross sections for the different ‘Higgs’ coupling operators, normalized to the acceptance cuts Eq.(17).

be avoided because they reduce the number of observables available for the analysis of the Higgs coupling structure. For the remaining part of this paper we will only apply Eqs.(17) and (18).

This reduced set of kinematic cuts has an effect on the distinguishing power of the observable  $\Delta\phi_{jj}$ . Forcing the two tagging jet into a more collinear configuration enhances the modulation for example distinguishing the three scalar coupling structures [11, 20]. However, we will see that  $\Delta\eta_{jj}$  itself is a powerful observable distinguishing coupling structures, so this effect can better be exploited through a two-dimensional  $\Delta\phi_{jj}$  vs  $\Delta\eta_{jj}$  analysis.

### A. Tagging jet kinematics

From the WBF analyses [28, 29] we know what the kinematic features of the two tagging jets and the heavy SM Higgs boson are: both tagging jets are distinctively forward and there is only little color activity between them [37], except for final state radiation off the centrally produced Higgs boson. All of this we show in Fig. 7. The corresponding distributions for the coupling structures  $0_{D5}^+$  and  $0_{D5}^-$  are very similar, with a slight difference due to the absence of the longitudinal amplitude for the  $0^-$  coupling. In the spin-2 case with couplings only to weak gauge bosons,  $2_{EW}^+$ , the tagging jets are more central. Also including graviton emission from quark lines,  $2_{EW+q}^+$ , shifts the tagging jets into the forward region. This effect is a first indication that for a spin-2 interpretation of the Higgs-like resonance the details of the underlying model have a significant effect on essentially all observables. A complete set of reference distributions is shown in Fig. 14 in the Appendix.

Another serious issue arises when we compare the transverse momentum distributions of the tagging jets (or the recoiling heavy resonance). The momentum dependence of the spin-2 coupling generates  $p_{T,j}$  spectra extending beyond a TeV. However, consistent models of a spin-2 resonance will include an additional form factor to cut off this tail and render all  $p_T$  distributions more similar to the scalar case [35]. Including distributions with an energy dimension, like the transverse momentum of the tagging jets and the central resonance will only test different implementations of such a form factor which cannot be derived from first principles.

The same behavior can be observed in WBF production of heavy  $W'$  bosons, for example in little Higgs models [34]. Just introducing additional heavy gauge bosons appears to predict very large momenta of the tagging jets. However, for heavy gauge bosons we can also check a consistent theory including heavy fermion partners and indeed find  $p_{T,j}$  distributions very similar to the known Higgs case. To test the stability of or results with respect to the UV completion of the spin-2 model we also show results requiring the tagging jets to fulfill

$$p_{T,j} < p_T^{\max} = 100 \text{ GeV} . \quad (20)$$

The starting point of our analysis of ‘Higgs’ coupling structures in weak boson fusion is the azimuthal angle between the two tagging jets [11]. Its relation to alternative observables we discuss in Sec. IIB and specifically in Fig. 2, indicating that it should be well suited to distinguish different spin-0 and spin-2 hypotheses.

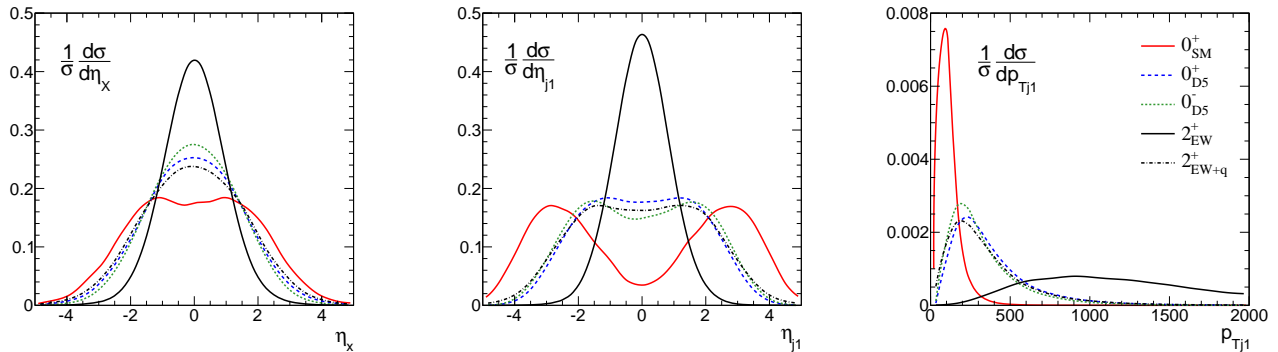


Figure 7: Rapidity of the resonance  $X$  (left), rapidity of the leading tagging jet (center), and transverse momentum of the leading tagging jet (right) for the different spin-0 and spin-2 hypotheses after the cuts of Eqs.(17) and (18). The hypotheses  $0_{SM}^+$  (red),  $0_{D5}^+$  (blue dashed),  $0_{D5}^-$  (green dashed),  $2_{EW}^+$  (black), and  $2_{EW+q}^+$  (black dashed) are defined in Tab. I.

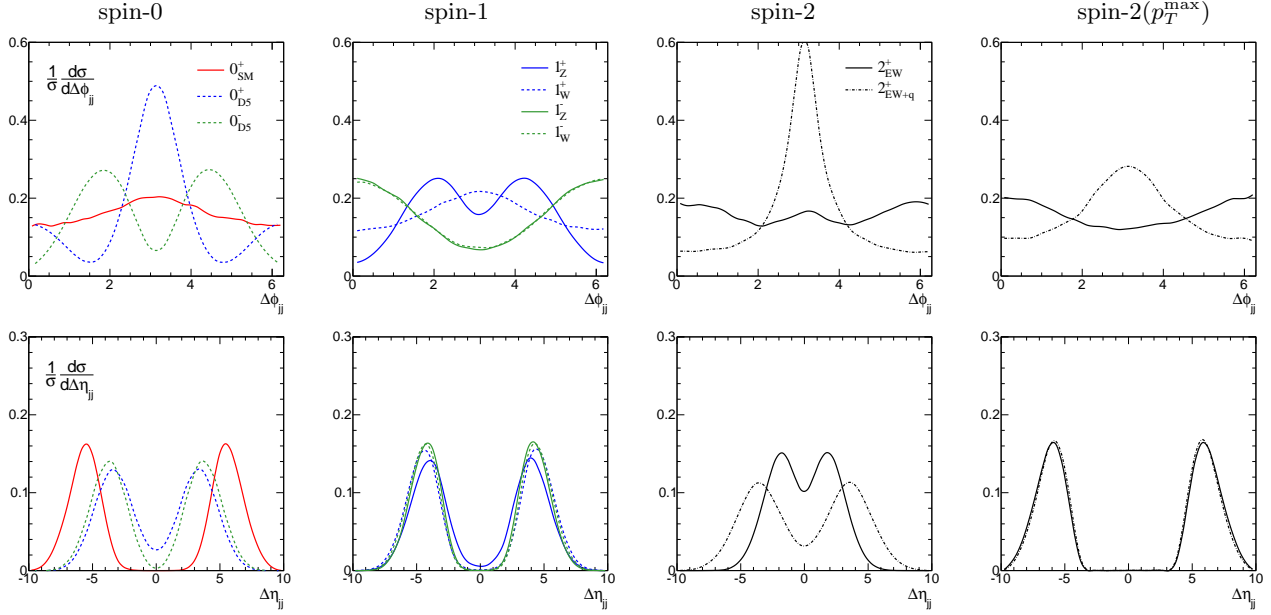


Figure 8: Normalized correlations between the two tagging jets in WBF production of a heavy resonance  $X$ . We show the difference in the azimuthal angle  $\Delta\phi_{jj}$  and the rapidity difference  $\Delta\eta_{jj}$ . The spin-0, spin-1, spin-2 interaction structures are described in Tab. I:  $0_{\text{SM}}^+$  (red),  $0_{\text{D5}}^+$  (blue dashed),  $0_{\text{D5}}^-$  (green dotted);  $1_Z^+$  (blue),  $1_W^+$  (blue dashed),  $1_Z^-$  (green),  $1_W^-$  (green dashed);  $2_{\text{EW}}^+$  (black),  $2_{\text{EW}+q}^+$  (black dashed). For the spin-2 case we also show the distributions after requiring  $p_T^{\text{max}} = 100$  GeV (right panels).

In the upper panels of Fig. 8 we show the  $\Delta\phi_{jj}$  distributions for the nine different couplings listed in Tab. I. There are essentially four different patterns in the left three panels: a flat  $\Delta\phi_{jj}$  behavior ( $0_{\text{SM}}^+$ ,  $1_W^+$ ,  $2_{\text{EW}}^+$ ), a back-to-back peak at  $\Delta\phi_{jj} \sim \pi$  ( $0_{\text{D5}}^+$ ,  $2_{\text{EW}+q}^+$ ), a preferred angle around  $\pi/2$  ( $0_{\text{D5}}^-$ ,  $1_Z^+$ ), and preferably aligned tagging jets  $\Delta\phi_{jj} \sim 0$  ( $1_{W,Z}^-$ ). Due to the absence of the longitudinal amplitude for the  $0_{\text{D5}}^-$  operator we know that its distribution follows a  $1 - \cos 2\Delta\phi_{jj}$  modulation. On the other hand,  $0_{\text{D5}}^+$  follows a  $\cos \Delta\phi_{jj}$  shape from the interference between the transverse and longitudinal amplitudes [12].

The issue with the proper definition of the spin-2 couplings also appears in this azimuthal observable. First, the distributions without ( $2_{\text{EW}}^+$ ) and with ( $2_{\text{EW}+q}^+$ ) a coupling to quarks have little in common. Secondly, removing the high-energy tale of the jet momenta requiring Eq.(20) strongly affects the full spin-2 distribution  $2_{\text{EW}+q}^+$ , changing it from distinctively peaked at  $\Delta\phi_{jj} = \pi$  to essentially identical to the Standard Model Higgs scalar  $0_{\text{SM}}^+$ . This is a general feature which we can trace back to the helicities probed by the spin-2 amplitude: once we limit it to relatively small energies of external particles it probes exactly the same helicity structure as the spin-0 Standard Model operator [12].

In the lower panels of Fig. 8 we show the rapidity difference  $\Delta\eta_{jj}$  between the two tagging jets. In the standard WBF analyses we require  $\Delta\eta_{jj} > 4.2$ , cutting away most of the spin-1 and spin-2 events and keeping mostly the Standard Model Higgs  $0_{\text{SM}}^+$  events. Skipping this cut we see that there are three distinct groups of curves, with maxima around  $\Delta\eta_{jj} \sim 2$  ( $2_{\text{EW}}^+$ ),  $\Delta\eta_{jj} \sim 4$  ( $0_{\text{D5}}^+$ ,  $1_W^+$ ,  $2_{\text{EW}+q}^+$ ), and  $\Delta\eta_{jj} \sim 5.5$  ( $0_{\text{SM}}^+$ ). Asking for tagging jets with limited energy, Eq.(20), turns both spin-2 distributions into an exact copy of the  $0_{\text{SM}}^+$  predictions. In this case only two distinctly different patterns survive, SM-Higgs-like and slightly less forward.

These rapidity differences are strongly correlated with the tagging jet rapidities shown in Fig. 7. Only very little information remains in the additional observation of  $\eta_{j,1}$  once we exploit  $\Delta\eta_{jj}$ . This is an effect of the WBF ansatz we are using for all resonances hypotheses — if any of the processes under consideration included a mixed quark-gluon initial state the boost from the laboratory frame to the center-of-mass frame of the two tagging jets might well turn out useful.

The main advantage of the two observables discussed in this section is that they do not require the reconstruction of the heavy resonance. In Sec. IV E we will compare the two observables  $\Delta\phi_{jj}$  and  $\Delta\eta_{jj}$  in their distinguishing power testing some spin-0 and spin-2 coupling structures. A complete set of distributions can be found in Fig. 15 in the Appendix. As expected, the study of decay independent jet correlations is a very useful starting point for a ‘Higgs’ coupling analysis [11]. However, the predictions from a spin-2 model have to be

taken with a grain of salt, because they are not stable with respect to (slight) modifications of the underlying model.

### B. Higgs-jet correlations

Adding information on the ‘Higgs’ momentum requires the reconstruction of the heavy resonance. This means that the most promising channel for such an analysis would be the decay  $X \rightarrow \gamma\gamma$ , possible supplemented by the approximate reconstruction of  $X \rightarrow \tau\tau$  decays. The latter requires additional assumptions about the couplings of the heavy resonance to fermions. This is most obvious in the spin-1 case, where in Eq.(13) we assume that the heavy neutral resonance couples to the third generation in complete analogy to a Standard Model  $Z$  boson.

This kind of assumption has for a long time been a problem in the interpretation of  $Z'$  searches, so it would be beneficial if we could apply an analysis of the coupling structure without considering fermionic couplings. Similarly, for WBF Higgs production the spin-2 states coupling to the energy-momentum tensor makes specific assumptions about the production vertex and about the decay vertex. It would be preferable if these two assumptions could be kept separate.

A way of including significantly more information than just the jet-jet correlations discussed in the previous section and at the same time making minimal assumptions about the decay of the heavy resonance is to study angular correlations between the tagging jets and the reconstructed resonance  $X$ . In this second step of the angular analysis we will focus on the observables  $\Delta\eta_{jX}$  and  $\Delta\phi_{jX}$ , where  $j$  denotes the tagging jet with the larger transverse momentum. This ordering of the tagging jets induces a difference compared to the Breit-frame analysis described in Sec.II A, where the tagging jets are ordered by rapidity.

In the upper panels of Fig.9 we show the rapidity difference between the reconstructed heavy resonance and the leading tagging jet. As expected from the tagging jet distributions shown in Sec. IV A the Standard Model Higgs  $0_{SM}^+$  is peaked at large differences  $\Delta\eta_{jX} \sim 2$ . The unitarized spin-2 resonance has a characteristically flat behavior. The  $\Delta\eta_{jX}$  distributions for all spin-1 coupling structures as well as the dimension-5 scalars are only marginally distinctive.

The second set of panels shows the azimuthal distance between the leading tagging jet and the heavy resonance. The Standard Model Higgs and the cut-off  $2_{EW}^+$  structures predict the same moderate back-to-back topology. For spin-1 the  $1_V^-$  and  $1_W^+$  distributions are much more strongly peaked in the same back-to-back kinematics.

Comparing the jet- $X$  correlations shown in Fig. 9 with the jet-jet correlations from Fig. 8 clearly shows that

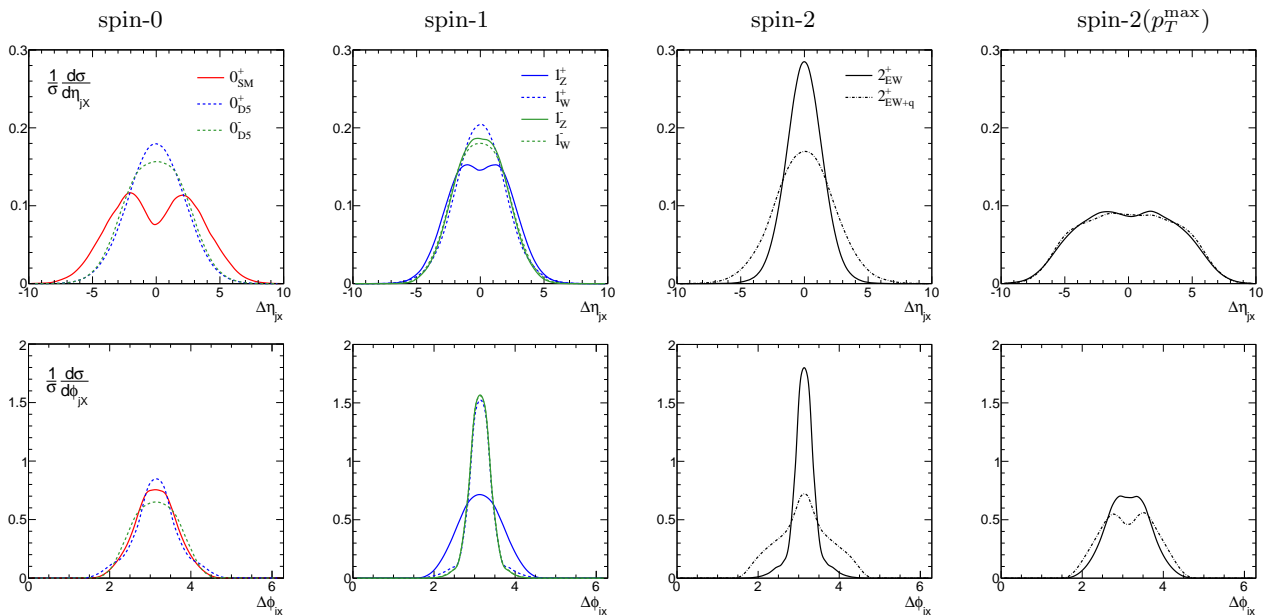


Figure 9: Normalized correlations between the leading tagging jet and the heavy resonance. We show the difference in the rapidity difference  $\Delta\eta_{jX}$  as well as the azimuthal angle  $\Delta\phi_{jX}$ . The spin-0, spin-1, spin-2 interaction structures are described in Sec. III A-III C.

in weak boson fusion the spin and coupling information is largely encoded in the tagging jets, not in the angular correlations of the heavy resonance [11], with the notable exception of a unitarized spin-2 model [12].

### C. Including Higgs decays

Essentially all information on the Higgs couplings structure available from ‘Higgs’ production in weak boson fusion is included in the jet-jet and jet- $X$  correlations described in the previous two sections. The only caveat is that the resonance observed in the final state might have a spin or polarization structure which we average over unless we make certain requirements on the  $X \rightarrow d\bar{d}$  decay products. The price we have to pay for this additional information is a full simulation of the  $X$  decay, including its underlying coupling structure. If we limit ourselves to  $VVX$  couplings for the production process this obviously implies additional assumptions for all decays except for decays to massive weak gauge bosons  $X \rightarrow VV$ . Moreover, the production and decay process  $VV \rightarrow X \rightarrow VV$  requires a unitarization which only the  $0_{\text{SM}}^+$  delivers and which we have to add for example for a spin-2 resonance. In Fig. 7 we see that this unitarization has a major effect on all energy dependent distributions, which means we have to take the jet-decay correlations with a grain of salt.

Nevertheless, in Fig.10 we show the usual rapidity and azimuthal angle differences between the leading tagging jet and one of the two  $X$  decay products. For the decay channel we assume  $X \rightarrow \tau^+\tau^-$  with the couplings described in Sec. III. Comparing these distributions to the jet- $X$  distributions in Fig. 9 we see that their features are very similar, *i.e.* the heavy resonance decay kinematics is dominated by the jet- $X$  kinematics. Small effects come from the acceptance cuts for the decay products. The main target for production-decay correlations is the spin-2 hypothesis, which after the unitarization cut  $p_{T,j} < p_T^{\text{max}}$  in Eq.(20) tends to be dominated by the helicity-2 states.

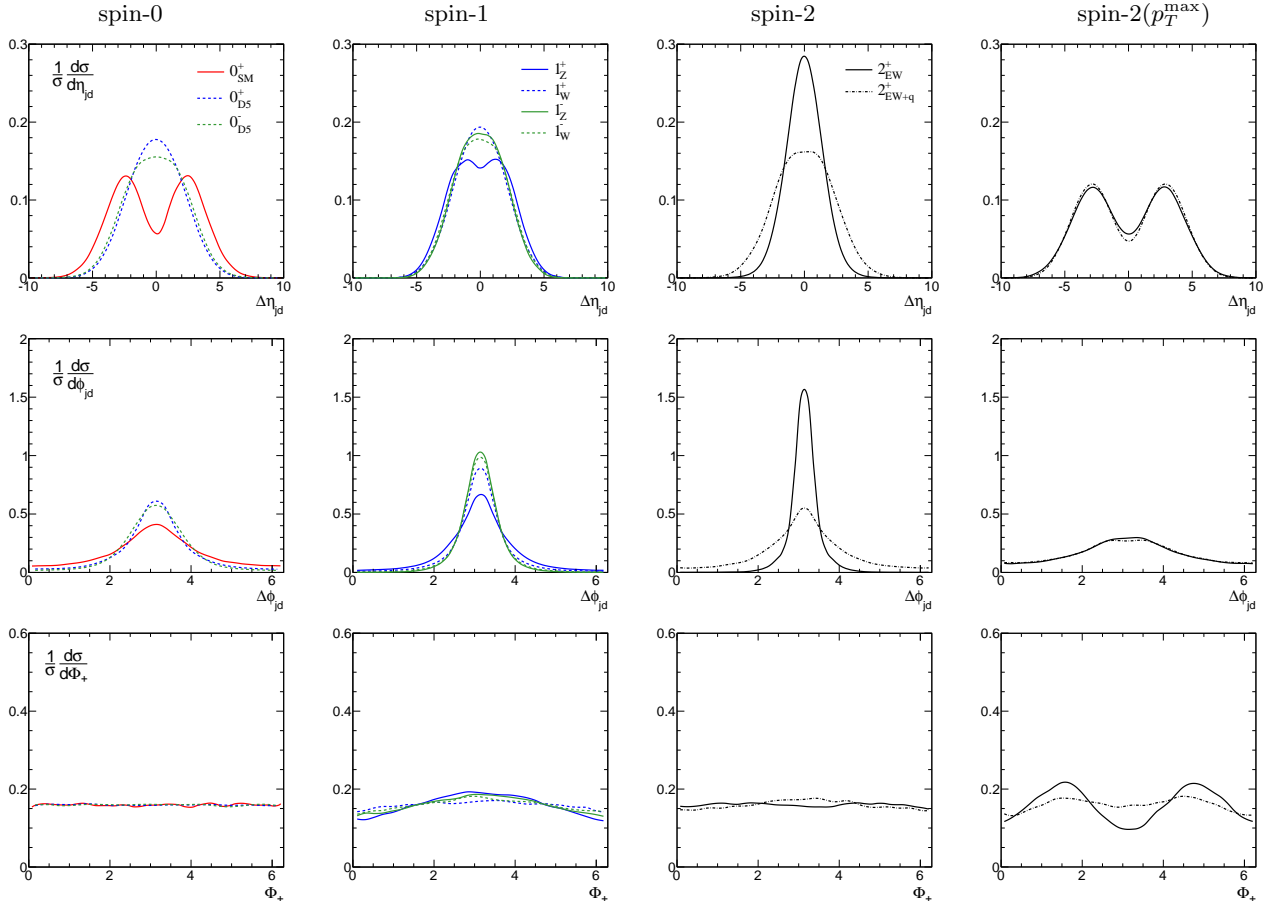


Figure 10: Normalized correlations between the leading tagging jet and the  $X$  decay particle. We show the difference in the rapidity difference  $\Delta\eta_{jd}$  as well as the azimuthal angle  $\Delta\phi_{jd}$ . In the bottom row we show the angle  $\Phi_+$  in the Breit frame.



The spin-2 operator coupling to gauge bosons and to quarks is the only scenario where  $\Delta\eta_{jd}$  differs from  $\Delta\eta_{jX}$ . While the latter shows a centrally flat behavior, distinctively different from  $2_{\text{EW}}^+$  and  $0_{\text{SM}}^+$ , the distributions including the decay becomes much more similar to those. In this case the jet-decay correlations are even less useful than the jet- $X$  correlations. The  $\Delta\phi_{jd}$  distributions also resemble their  $\Delta\phi_{jX}$  counter parts closely, with a generic smearing because the tagging jets now recoil against to decay products instead of one resonance. Again, one change is that the two spin-2 hypotheses are becoming indistinguishable, but possibly more different from the spin-0 predictions. Moreover, one exception to the general broadening of  $\Delta\phi_{jd}$  is the  $1_Z^+$  operator, which becomes more similar to the other spin-1 scenarios and less similar to the scalar couplings.

In addition to the generic hadron collider observables there are a few variables which are particularly well suited to identify a spin-2 resonance. One example is the Gottfried–Jackson angle [31, 32], which is very closely related to  $\cos\theta^*$  in the Breit frame. We show the corresponding distributions in the Appendix. In the bottom row of Fig. 10 we show the distribution of the angle  $\Phi_+ \equiv 2\phi_1 + \Delta\phi$  in the Breit frame [12], whose angles are defined in Eq.(4). Its particular feature is that it has no distinguishing features unless we unitarize the spin-2 rate, in which case it develops a clear modulation for spin-2 couplings. In principle the same information should be included in an appropriate combination of hadron collider observables, but it cannot be easily observed in combinations like  $\Delta\phi_{j1d} + \Delta\phi_{j2d}$ .

#### D. Basic strategy

From the discussion of the different jet-jet, jet- $X$ , and jet-decay observables we know that there are a few key measurements which can distinguish between the ‘Higgs’ coupling structures. The hadron collider observables  $\Delta\eta$  and  $\Delta\phi$  serve as effective replacements of the Cabibbo–Maksymowicz–Dell’Aquila–Nelson angles [13, 14]. A particular strength of the angular basis for  $X \rightarrow ZZ$  decays is the clear link between some of some Higgs couplings structures and particular distinctive observables. The distribution of the azimuthal angle  $\Delta\phi_{jj}$  [11] shown in Fig. 2 constitutes such a specific link in the WBF topology.

Hence, the question arises if we can construct a set of measurements which can distinguish the different ‘Higgs’ operators shown in Tab. I. Such a simple flow diagram does not correspond to an optimized experimental analysis, but it indicates what the key observables are. For example, from Sec. IV we know that we should avoid cutting on  $\Delta\eta_{jj}$  before testing ‘Higgs’ couplings because it removes one of the key observables to tell apart the  $0_{\text{D5}}^+$  and  $0_{\text{SM}}^+$  operators. Following our earlier argument we do not include the transverse momentum spectrum of the tagging jets in our list of observables because the initially striking differences will be modified by form factors for spin-1 and spin-2 resonances. For now, we consistently assume spin-2 operators with our simplified unitarization cut  $p_T^{\text{max}} = 100$  GeV as defined in Eq.(20). Without this cut a spin-2 could be immediately recognized from the  $p_T$  spectra shown in Sec.IV A.

In Fig. 11 we show some of the most distinctive measurements reflecting the couplings of a heavy resonance. The first jet-jet variable,  $\Delta\phi_{jj}$ , is well suited to clearly separate the spin-0 structures. As we will see in the following section the  $\Delta\eta_{jj}$  distribution might be even more powerful than  $\Delta\phi_{jj}$ , so there should be no problem in distinguishing the different spin-0 structures just based on the tagging jets.

The problem is to tell apart some of the spin-1 and spin-2 hypotheses from their closest spin-0 models in the jet-jet correlations. For example, to tell apart the Standard Model Higgs boson  $0_{\text{SM}}^+$  and the graviton  $2_{\text{EW+q}}^+$  we have to resort to the jet- $X$  correlations  $\Delta\eta_{jX}$ . From Sec. IV C we know that Breit frame angles would also be well suited for this distinction, most notably  $\Phi_+$  [12].

Similarly, telling apart  $0_{\text{D5}}^-$  and  $1_Z^+$  we requires jet-decay correlations like  $\Delta\eta_{jd}$ . Alternatively, we could use  $\Phi_+$  shown in Fig. 10, the Breit-frame angle  $\theta^*$ , or the Gottfried–Jackson angle  $\theta_{\text{GJ}}$ . The two operators  $1_{W,Z}^-$  appear indistinguishable using the set of observables at hand.

The qualitative bottom line of this section is that clearly the jet-jet correlations are the most decisive, in particular to separate the different scalar coupling structures [11]. For some spin-1 and (unitarized) spin-2 models we need to add information from the heavy resonance or its decays [12].

#### E. Comparison of observables

Following Sec. IV D we know what the candidate observables for the distinction of model hypotheses are. However, for example for the distinction of the  $0_{\text{SM}}^+$  and  $0_{\text{D5}}^+$  coupling structures there are several such variables. Only a complete shape analysis can tell us how promising these distributions really are.

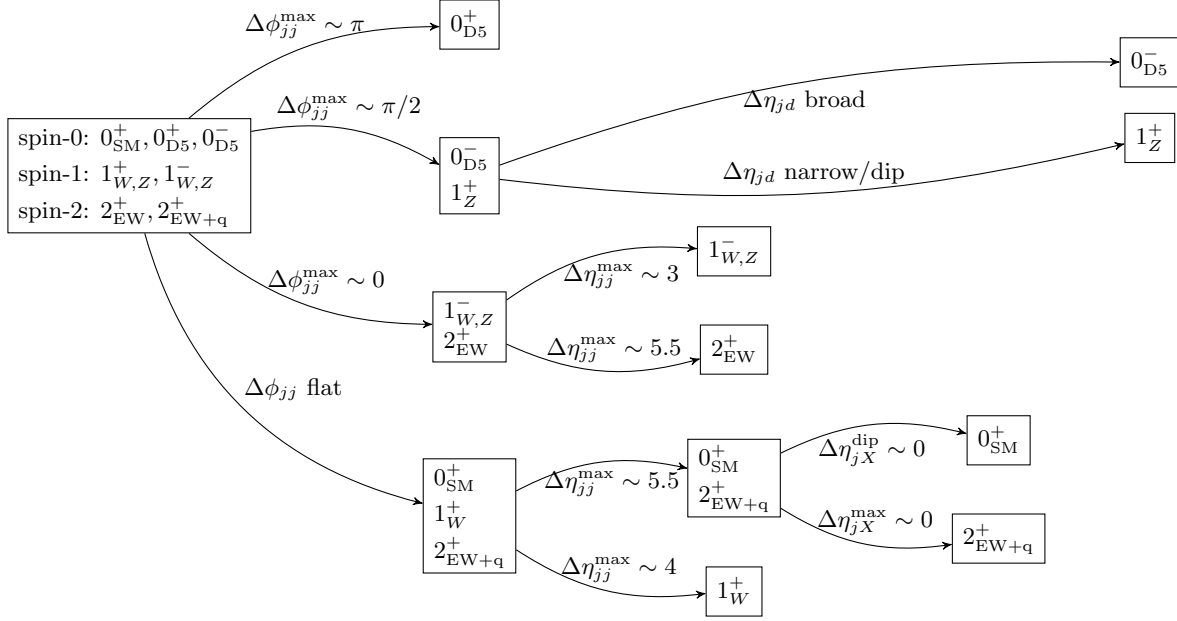


Figure 11: Flow diagram for testing Higgs coupling structure in WBF production. All spin-2 models are defined including the unitarization cutoff Eq.(20).

The statistical power of a well-defined set of observables we compute based on statistical errors, ignoring systematics as well a theoretical uncertainties and errors. This approximation is justified for relatively low luminosities — for example asking the question which of the distributions would first cross a given confidence level in the comparison between two hypotheses.

To asses such a minimal luminosity we perform a binned log-likelihood ratio hypothesis test [47]. Our zero hypothesis or background hypothesis is the Standard Model coupling structure  $0_{\text{SM}}^+$ . This hypothesis also fixes the number of events in the distribution. The exotic signal we would like to discover or reject are the alternative spin-0 or spin-2 coupling structures. Backgrounds we ignore in this computation, because they mostly affect the exact value of the luminosity required for a 95% exclusion, but not the relative strength of the different observables. The binned likelihood is defined in terms of a Poisson likelihood  $L$ ,

$$L(\text{data} | \text{hypothesis } X) = \frac{N^n(X) e^{-N(X)}}{n!}$$

$$\mathcal{Q} = -2 \log \frac{L(\text{data} | \text{hypothesis } 1)}{L(\text{data} | \text{SM})} . \quad (21)$$

The expected number of signal events (per bin) given the luminosity  $\mathcal{L}$  is  $N(X) = \sigma(X)\mathcal{L}$ , while  $n$  is the observed number of signal events. The logarithm is additive, so the generalization of Eq.(21) to binned distributions with (in our case) 20 bins per distribution is straightforward. The Neyman–Pearson lemma states that this is the statistically ‘best’ discriminator. The different hypotheses in Eq.(21) are sampled with randomly generated pseudo-data, giving us probability density functions whose overlap define the 95% CL curves. As alluded to above, the absolute value of the luminosity required for a 95% CL exclusion of alternative coupling structure should be taken with a grain of salt. What we aim at is the relative strength of the different observables, which might be hard to judge by eye.

In Fig. 12 we compare the statistical power of different observables in WBF kinematics. In the left panel we show how well the different observables can distinguish the  $0_{\text{D5}}^+$  operator from the Standard Model coupling structure. The two most promising observables are the rapidity difference between the two tagging jets and their azimuthal angle difference, *i.e.* observables which are independent of the Higgs decay. All that is required is that the event sample has a good signal-to-background ratio, such that such an analysis is not dominated by the systematics of the background subtraction. The necessary clean-up of the event sample can be achieved by central jet vetos [37] and/or the matrix element method [30]. We see that the rapidity difference turns out more powerful than the azimuthal angle.

In the second panel we show the same set of observables for a discovery of the CP-odd  $0_{\text{D5}}^-$  coupling structure, a pseudo-scalar Higgs boson. Again, the azimuthal angle  $\Delta\phi_{jj}$  is somewhat less sensitive compared to the rapidity

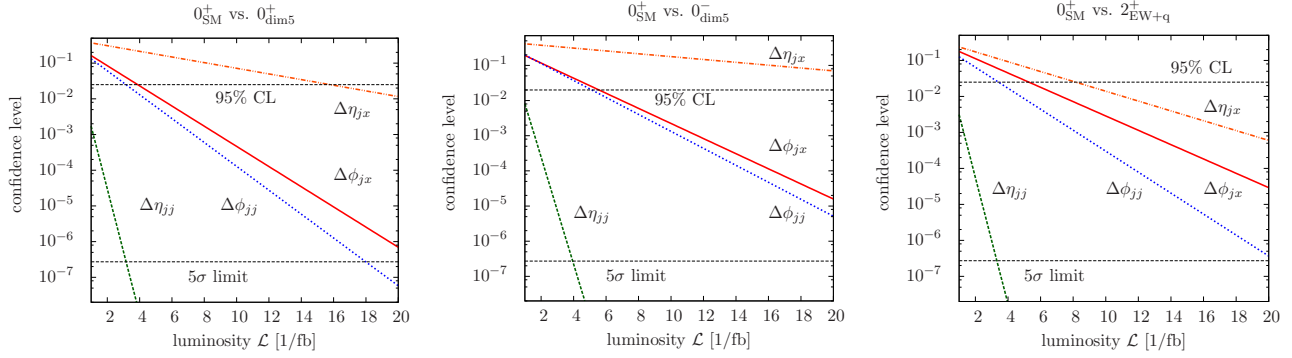


Figure 12: Confidence level for the distinction of different spin-0 coupling structures as a function of the integrated luminosity. We assume statistical uncertainties only for the WBF signal in the absence of backgrounds. The plotted confidence level refers to exclusion of the SM WBF component. The cross section normalization is 2.8 fb which corresponds to a good  $\tau$  reconstruction in the purely leptonic channels (see [19]).

difference. Finally, we study the most relevant observables to identify a  $2^+$  resonance without a constraint on the high-energy tails of the jet momenta. As before, the rapidity difference of the tagging jets is the most powerful. These results are a direct consequence of the high discriminative power of the  $\Delta\eta_{jj}$  distribution shown in Fig. 8, where all the alternative couplings tested in this section peak around  $\Delta\eta_{jj} \sim 4$ , compared to the Standard Model  $0_{SM}^+$  case with  $\Delta\eta_{jj} \sim 5.5$ . For spin-2 identification adding information from the heavy resonance or its decays implies a significant improvement [12]. Our results for the best-suited distribution reflects the setup of the likelihood test: the required luminosity is dominated by those bins which show a large ratio of events between the two different hypotheses.

Going beyond our idealized setup, these jet-jet observables differ when it comes to detector and QCD effects, e.g. pile-up suppression is a function of rapidity. Furthermore it is well-known that  $\Delta\phi_{jj}$  acts as good measurement quantity to extract mixed CP properties [20]. Such an angular correlation is insufficiently reflected in the rapidity difference. This way  $\Delta\phi_{jj}$  remains a well-suited observable to test more complex CP properties in WBF Higgs production, while a wide operator spectroscopy preferably relies on the leading observable  $\Delta\eta_{jj}$ .

## V. ZH PRODUCTION

The study of WBF kinematics with the different decay channels gives us a wide array of tests of the Higgs coupling structures. However, fermions still only feature in one channel, namely  $X \rightarrow \tau^+\tau^-$  decays. Once the LHC runs at 14 TeV, another channel will become available to test the ‘Higgs’ couplings to fermions,

$$pp \rightarrow (Z \rightarrow \ell^+\ell^-)(X \rightarrow b\bar{b}) . \quad (22)$$

Independent of the use of modern Higgs finding methods [24] this channel will only be observable for boosted  $Z$  and  $X$  decays. The kinematics of this process can be directly mapped onto the decay  $X \rightarrow ZZ$ , so the Cabibbo–Maksymowicz–Dell’Aquila–Nelson angles [13] are a natural choice for spin-sensitive observables. In complete analogy to Eq.(2) we define

$$p_{Z^*} = p_Z + p_X , \quad p_X = p_b + p_{\bar{b}} , \quad p_Z = p_{\ell^-} + p_{\ell^+} . \quad (23)$$

as well as the corresponding unit three-momenta  $\hat{p}_i$  in the  $Z^*$  and the  $Z, X$  rest frames. Similar to the original angles defined in Sec. II A the  $Z^*$  in the  $s$ -channel will be off-shell, which does not prevent us from using it as a reference frame. The basis of angles is then defined as

$$\begin{aligned} \cos \theta_b &= \hat{p}_{b_1} \cdot \hat{p}_Z \Big|_X & \cos \theta_\ell &= \hat{p}_{\ell^-} \cdot \hat{p}_X \Big|_Z & \cos \theta^* &= \hat{p}_X \cdot \hat{p}_{\text{beam}} \Big|_{Z^*} \\ \cos \phi_b &= (\hat{p}_{\text{beam}} \times \hat{p}_Z) \cdot (\hat{p}_Z \times \hat{p}_{b_1}) \Big|_X & \cos \Delta\phi &= (\hat{p}_b \times \hat{p}_{\bar{b}}) \cdot (\hat{p}_{\ell^-} \times \hat{p}_{\ell^+}) \Big|_{Z^*} . \end{aligned} \quad (24)$$

The signal distributions for the different  $X$  hypotheses are generated with the rough acceptance cuts

$$p_{T,b} \geq 20 \text{ GeV} \quad p_{T,\ell} \geq 10 \text{ GeV} \quad \Delta R \geq 0.4 \quad |\eta_b| \leq 5 \quad |\eta_\ell| \leq 2.5 , \quad (25)$$

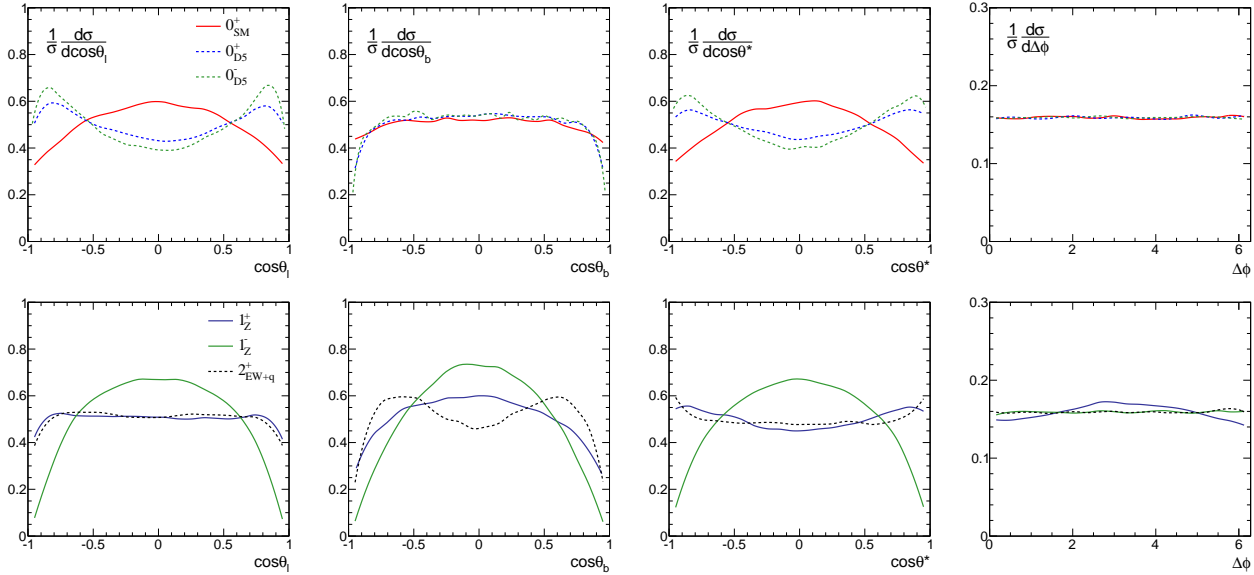


Figure 13: Angular correlations for  $(Z \rightarrow \ell^+\ell^-)(X \rightarrow b\bar{b})$  production. We show  $0_{\text{SM}}^+$  (red),  $0_{\text{D5}}^+$  (blue),  $0_{\text{D5}}^-$  (green),  $1_Z^+$  (blue) in the upper panels and  $1_Z^-$  (green), and  $2_{\text{EW}+q}^+$  (black dashed) in the lower panels. All operators are defined in Tab. I.

where we assume the same value for all  $\Delta R$  value for  $b$ -jets and leptons. In addition, we require

$$p_{T,(b\bar{b})} > 100 \text{ GeV} , \quad (26)$$

to be consistent with the proposed LHC analyses.

Because this analysis requires reconstructed  $Z \rightarrow \ell^+\ell^-$  and the  $H \rightarrow b\bar{b}$  decays we limit our model hypotheses from Tab. I to those which predict a  $XZZ$  coupling as well as a  $Xb\bar{b}$  coupling. For this sub-set of spin-0, spin-1, and spin-2 models we should the most discriminating distributions in Fig. 13. The three scalar operators can be identified by a flat  $\cos\theta_b$  distribution. The SM and the two higher-dimensional scalar couplings then show a distinctively different behavior in  $\cos\theta_\ell$ , which carries the same physical information as the  $\cos\theta_e$  distribution presented in Fig.3 for the  $X \rightarrow ZZ$  decay. The challenge in the scalar sector will be the measurement of the CP property of the  $0_{\text{D5}}^\pm$  operators. The problem with these two states is that they are both scalars, washing out any angular correlation between the  $X \rightarrow b\bar{b}$  and the  $Z \rightarrow \ell^+\ell^-$  decays. If their dimension-5 origin gives them a similar energy behavior we would need a dedicated CP asymmetry to distinguish them.

Comparing the different spin-1 and spin-2 hypotheses is made easy by the distinctive forward-backward peaks in the spin-2 prediction for  $\cos\theta_b$ . For  $\theta_\ell$  and  $\theta^*$  the  $1_Z^-$  distribution has a significantly larger preference for  $\cos\theta = 0$ . While the boosted kinematics might well start to wash out the angular correlations of the  $Z, X$  decay products, this simple set of predictions indicates that the determination of Higgs coupling structures in associated  $ZH$  production is promising.

## VI. OUTLOOK

After the discovery of a Higgs-like resonance by ATLAS and CMS the main focus of Higgs analyses at the LHC will be the determination of the Higgs Lagrangian. This includes the structure of the operators (linked to the spin and CP quantum numbers of the ‘Higgs’ boson) as well as an independent measurement of the coupling strength. Similar to the hugely successful electroweak precision program centered around LEP this should give us hints about the embedding of the Higgs mechanism in an ultraviolet completion of the Standard Model.

We present a comprehensive study for the determination of the Higgs coupling structure in weak boson fusion. Starting from the Cabibbo–Maksymowicz–Dell’Aquila–Nelson angles in  $X \rightarrow ZZ$  decays we show how the WBF kinematics can be described either using Breit frame angles or rapidity and azimuthal angles.

The most distinctive observables in the WBF topology are jet-jet correlations. It is well known that the azimuthal angle  $\Delta\phi_{jj}$  can distinguish between different spin-0 couplings without ever requiring a reconstructed

resonance momentum [11, 20]. Based on a signal-only and parton level statistical analysis we expect the rapidity difference  $\Delta\eta_{jj}$  to be at least as effective in distinguishing different spin-0 and spin-1 hypotheses. The advantage of jet-jet correlations is that we do not have to model ‘Higgs’ decays based on different models, where the production in weak boson fusion and a decay to photons or fermions might probe very different underlying assumptions on the production and decay sides.

Generalizing our analysis to spin-1 and spin-2 hypotheses requires additional information from the heavy resonance decays [12]. Again, the more general approach is to reconstruct the heavy resonance momentum without any assumption on the decay vertex and test angular jet- $X$  correlations. We find that they indeed allow for a distinction of spin-0 and spin-1 or spin-2 models. Adding decays of the heavy resonances and computing jet-decay correlations adds only little in terms of the hadron collider observables  $\Delta\eta$  and  $\Delta\phi$ .

Nevertheless, it might be useful to add dedicated angular correlations defined differently. This includes an analytically continuation of the  $X \rightarrow ZZ$  angles, or some Breit frame angles like  $\theta^*$  or  $\Phi_+$ .

For associated  $ZH$  production with fully reconstructed decays  $Z \rightarrow \ell^+\ell^-$  and  $X \rightarrow b\bar{b}$  we can immediately employ the  $X \rightarrow ZZ$  angles. It should be possible to confirm the  $0_{\text{SM}}^+$  coupling structure also in this channel without any problems.

### Acknowledgments

We would like to thank Mario Campanelli for suggesting the analysis of angular correlations in the  $ZH$  channel. CE acknowledges funding by the Durham International Junior Research Fellowship scheme and thanks Michael Spannowsky for helpful discussions. KM has been in part supported by the Concerted Research action ‘‘Supersymmetric Models and their Signatures at the Large Hadron Collider’’ and the Research Council of the Vrije Universiteit Brussel, and in part by the Belgian Federal Science Policy Office through the Interuniversity Attraction Pole P7/37.

### Complete set of observables

In Sections IV A, IV B, and IV C we show a selected set of observables which should allow us to determine the coupling structure of a heavy Higgs-like resonance in weak boson fusion. We largely rely on the hadron collider observables  $\Delta\eta$  and  $\Delta\phi$ , even though in Sec.II A we introduce Breit frame observables as well as dedicated angles like the Gottfried-Jackson angle. In this appendix we give a complete set of distributions for all model hypotheses listed in Tab I.

In Fig. 14 we start by giving the complete set of rapidity and transverse momentum distributions for the heavy resonance  $X$  and the leading tagging jet. In addition to the curves shown in Fig. 7 we also show the scalar and spin-2 couplings to incoming gluons, as defined in Tab. I.

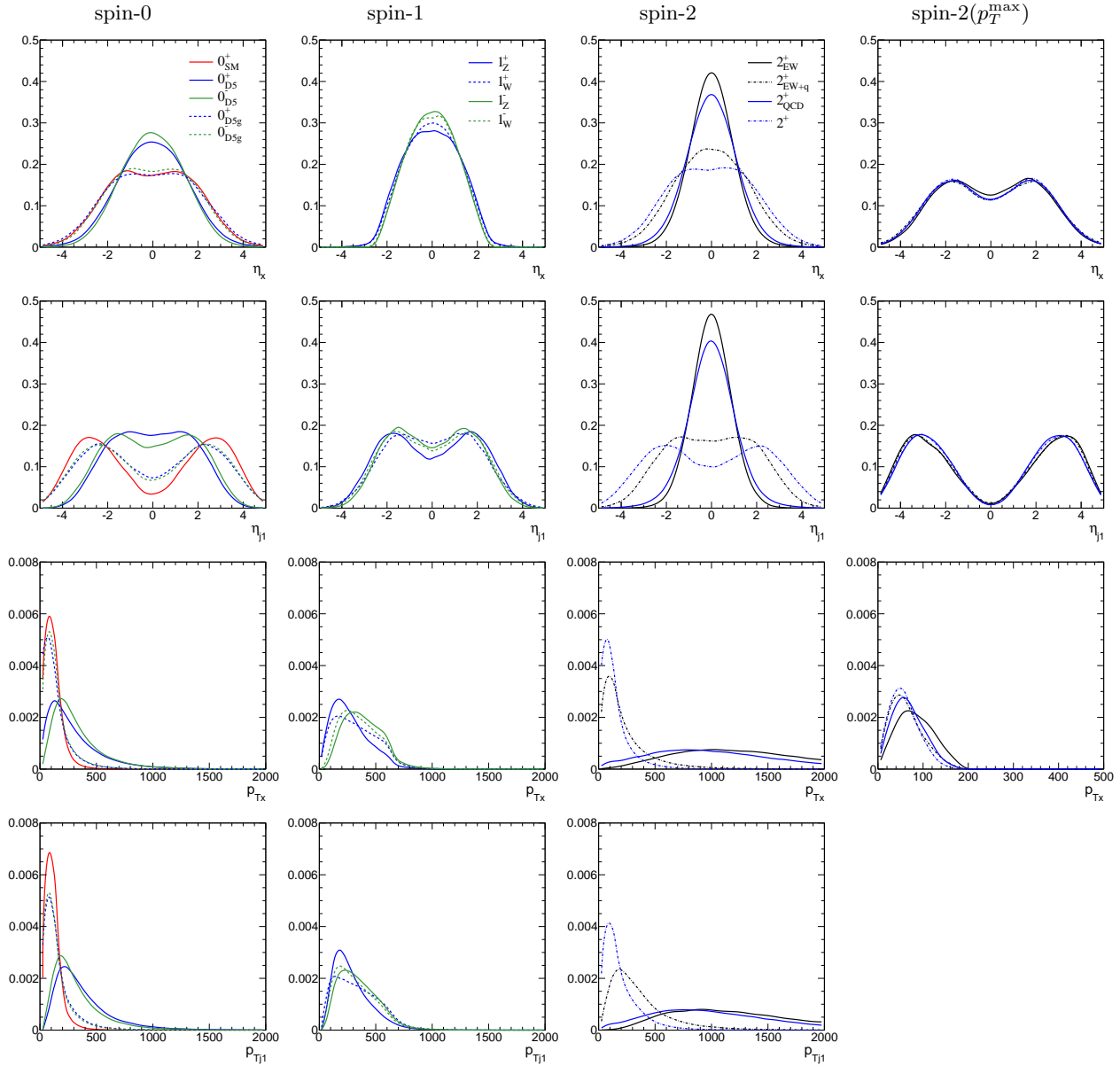


Figure 14: Normalized distributions of the heavy resonance  $X$  and the leading tagging jet after the minimal kinematical cuts of Eq.(17) and  $m_{jj} > 600$  GeV in Eq.(18). The hypotheses are  $0_{\text{SM}}^+$  (red),  $0_{\text{D5}}^+$  (blue),  $0_{\text{D5}}^-$  (green),  $0_{\text{D5(g)}}^+$  (blue dashed),  $0_{\text{D5(g)}}^-$  (green dashed);  $1_Z^+$  (blue),  $1_W^+$  (blue dashed),  $1_Z^-$  (green),  $1_W^-$  (green dashed);  $2_{\text{EW}}^+$  (black),  $2_{\text{EW+q}}^+$  (black dashed),  $2_{\text{QCD}}^+$  (blue),  $2^+$  (blue dashed), all defined in Tab. I.

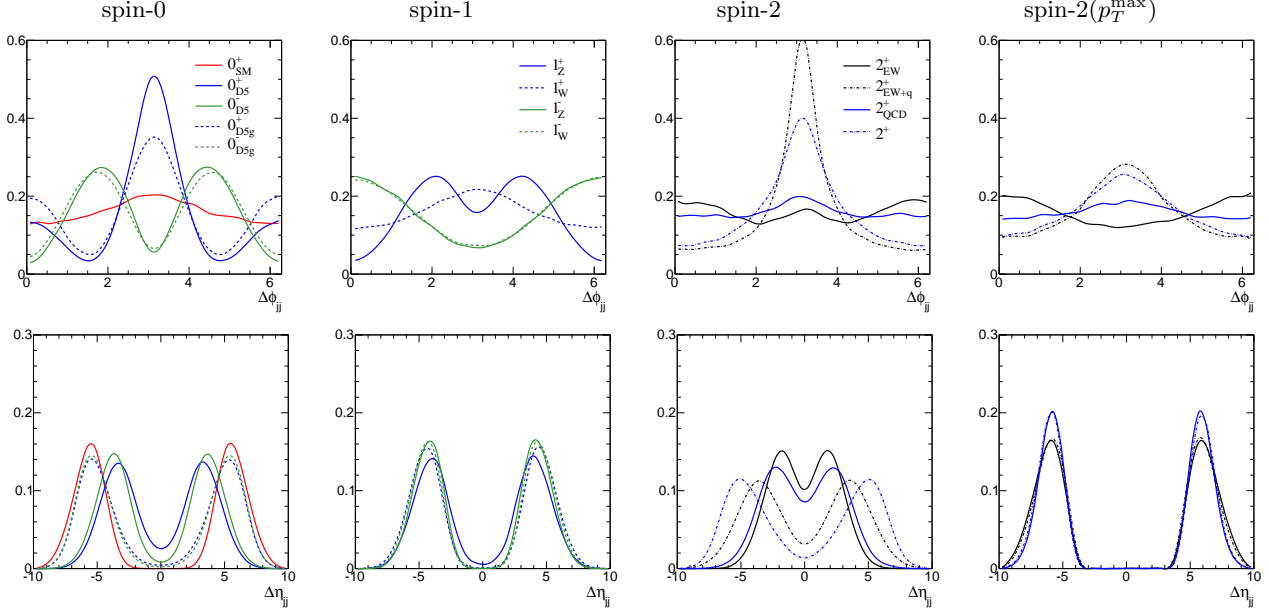


Figure 15: Correlations between the tagging jets. The different curves are the same as in Fig. 14.

In Figs. 15, 16, and 17 we show the jet-jet, jet- $X$ , and jet-decay correlations for the same full set of operators. This confirms the picture that comes out of Sec. IV, that for the WBF topology the jet-jet correlations are the most sensitive because they show the most distinctive kinematic patterns. Moreover, Fig. 15 confirms that adding a small fraction of gluon fusion events hardly changes or even dilutes the general features of the WBF kinematics. For all distributions we also observe a qualitative difference between the generic spin-2 couplings and the spin-2 couplings after a unitarization cut  $p_{T,j} = p_T^{\max}$ . A completely model independent test of spin-2 couplings is unfortunately not possible.

Finally, in Fig. 18 we show the most promising specific angular observable for the determination of the coupling structure in weak boson fusion. This includes the Breit-frame angles  $\Phi_+$  and  $\cos\theta^*$  defined in Eq.(4) as well as the Gottfried–Jackson angles introduced at the end of Sec. II A. We see that their benefit apart from a spin-2 identification is somewhat limited.

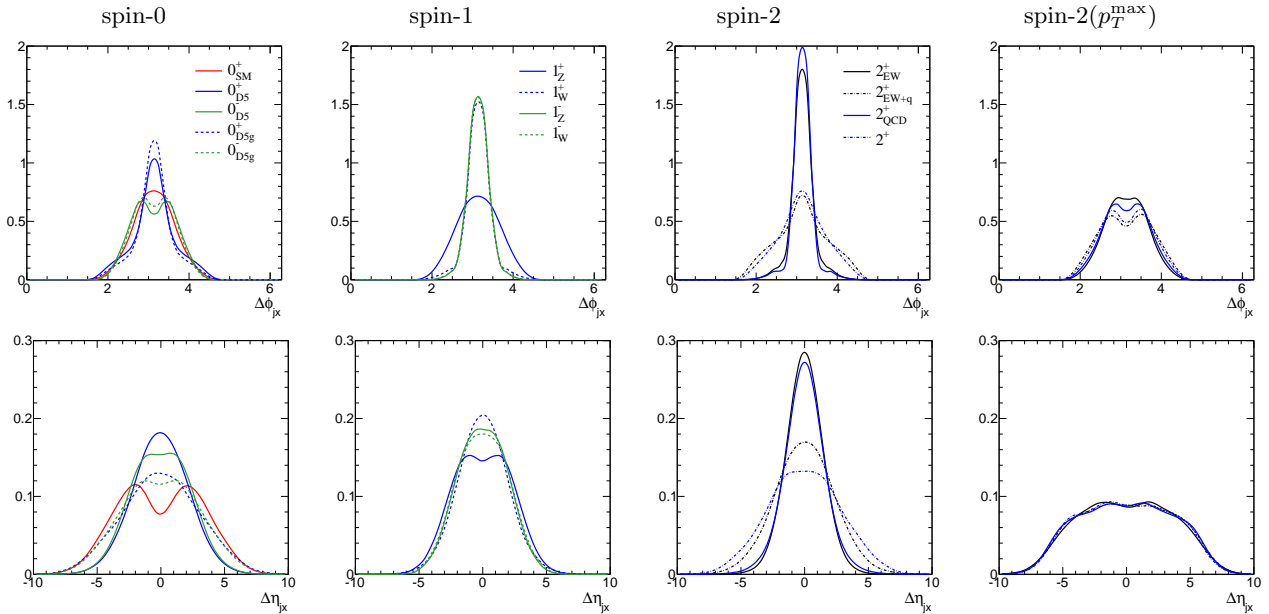


Figure 16: Same as Fig. 15, but among the heavy resonance  $X$  and the leading tagging jet.



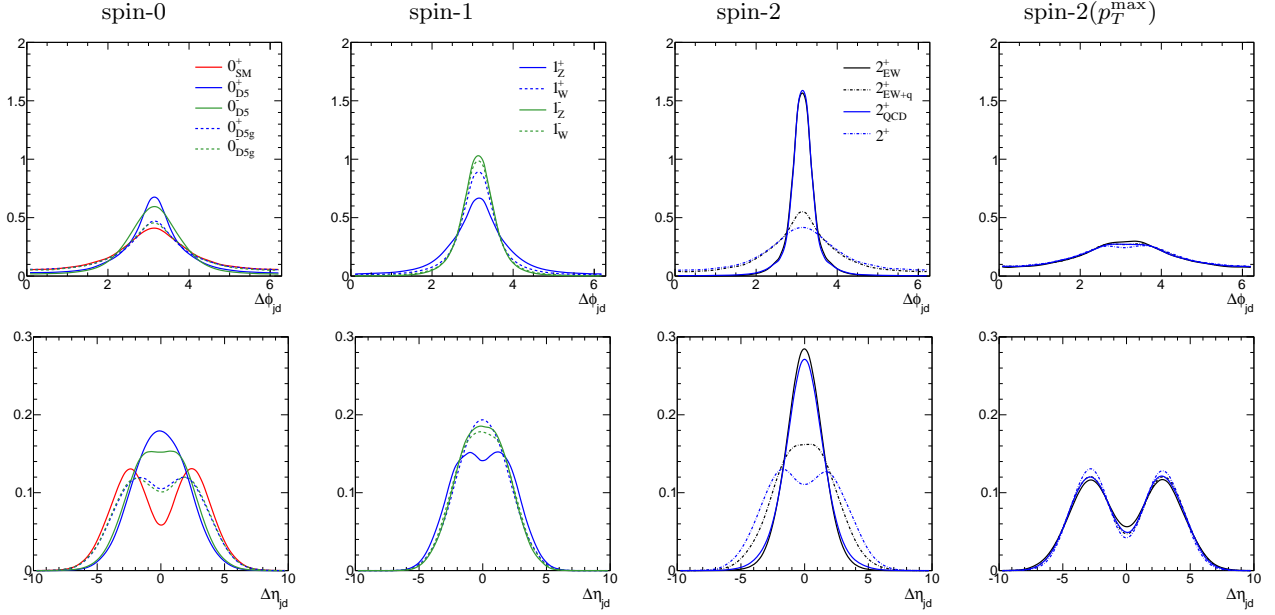


Figure 17: Same as Fig. 15, but among the leading tagging jet and the  $X$  decay products.

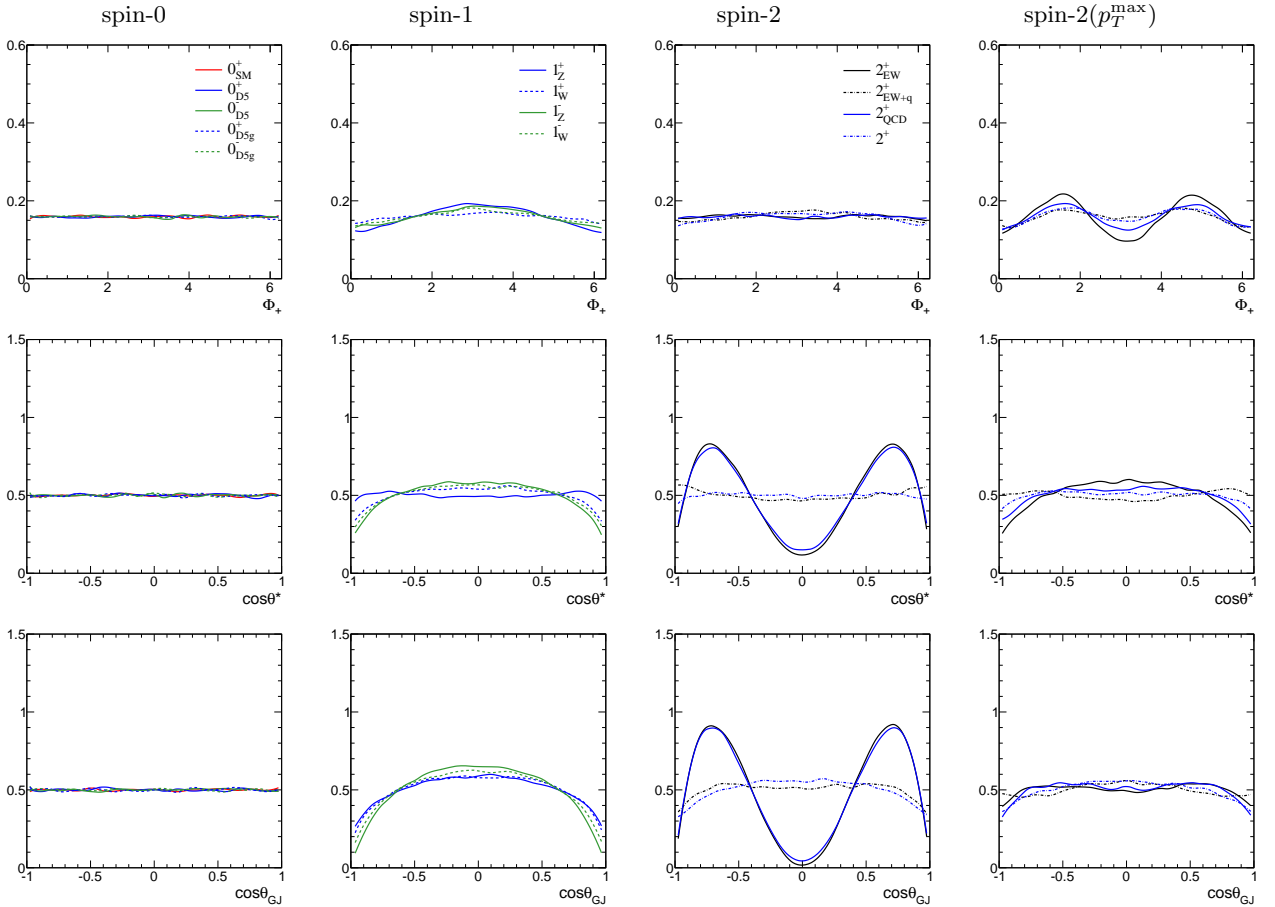


Figure 18: Specific angles targeted at identifying a spin-2 resonance. The different curves are the same as in Fig. 14.

- 
- [1] P. W. Higgs, Phys. Lett. **12**, 132 (1964); P. W. Higgs, Phys. Rev. Lett. **13**, 508 (1964); F. Englert and R. Brout, Phys. Rev. Lett. **13**, 321 (1964).
  - [2] G. Aad *et al.* [ATLAS Collaboration], Phys. Lett. B **716** (2012) 1.
  - [3] S. Chatrchyan *et al.* [CMS Collaboration], Phys. Lett. B **716** (2012) 30.
  - [4] The ATLAS collaboration, ATLAS-CONF-2012-158, ATLAS-CONF-2012-160, ATLAS-CONF-2012-161, ATLAS-CONF-2012-162, ATLAS-CONF-2012-163; The CMS collaboration, CMS-PAS-HIG-12-042, CMS-PAS-HIG-12-043, CMS-PAS-HIG-12-044, CMS-PAS-HIG-12-046, CMS-PAS-HIG-12-051.
  - [5] The CMS collaboration, CMS-PAS-HIG-12-041.
  - [6] M. Klute, R. Lafaye, T. Plehn, M. Rauch and D. Zerwas, Phys. Rev. Lett. **109**, 101801 (2012); T. Plehn and M. Rauch, Europhys. Lett. **100**, 11002 (2012).
  - [7] see *e.g.* A. Azatov, R. Contino and J. Galloway, arXiv:1202.3415; D. Carmi, A. Falkowski, E. Kuflik, T. Volansky and J. Zupan, arXiv:1207.1718; P. P. Giardino, K. Kannike, M. Raidal and A. Strumia, arXiv:1207.1347; J. Ellis and T. You, arXiv:1207.1693; J. R. Espinosa, C. Grojean, M. Mühlleitner and M. Trott, arXiv:1207.1717; A. Freitas and P. Schwaller, arXiv:1211.1980.
  - [8] The ATLAS collaboration, ATLAS-CONF-2012-127; The CMS Collaboration, CMS-PAS-HIG-12-045.
  - [9] T. Corbett, O. J. P. Eboli, J. Gonzalez-Fraile and M. C. Gonzalez-Garcia, Phys. Rev. D **86**, 075013 (2012); E. Masso and V. Sanz, arXiv:1211.1320; T. Corbett, O. J. P. Eboli, J. Gonzalez-Fraile and M. C. Gonzalez-Garcia, arXiv:1211.4580.
  - [10] for a pedagogical introduction see T. Plehn, Lect. Notes Phys. **844**, 1 (2012).
  - [11] T. Plehn, D. L. Rainwater and D. Zeppenfeld, Phys. Rev. Lett. **88**, 051801 (2002).
  - [12] K. Hagiwara, Q. Li and K. Mawatari, JHEP **0907**, 101 (2009).
  - [13] N. Cabibbo and A. Maksymowicz, Phys. Rev. **137**, B438 (1965) [Erratum-ibid. **168**, 1926 (1968)]; J. R. Dell'Aquila and C. A. Nelson, Phys. Rev. D **33**, 80 (1986); J. R. Dell'Aquila and C. A. Nelson, Phys. Rev. D **33**, 93 (1986); C. A. Nelson, Phys. Rev. D **37**, 1220 (1988).
  - [14] S. Y. Choi, D. J. Miller, M. M. Mühlleitner and P. M. Zerwas, Phys. Lett. B **553** (2003) 61; S. Y. Choi, M. M. Mühlleitner and P. M. Zerwas, arXiv:1209.5268.
  - [15] Y. Gao, A. V. Gritsan, Z. Guo, K. Melnikov, M. Schulze and N. V. Tran, Phys. Rev. D **81**, 075022 (2010); S. Bolognesi, Y. Gao, A. V. Gritsan, K. Melnikov, M. Schulze, N. V. Tran and A. Whitbeck, arXiv:1208.4018 [hep-ph].
  - [16] A. De Rujula, J. Lykken, M. Pierini, C. Rogan and M. Spiropulu, Phys. Rev. D **82**, 013003 (2010).
  - [17] C. P. Buszello, I. Fleck, P. Marquard and J. J. van der Bij, Eur. Phys. J. C **32** (2004) 209.
  - [18] C. Englert, C. Hackstein and M. Spannowsky, Phys. Rev. D **82** (2010) 114024.
  - [19] C. Englert, M. Spannowsky and M. Takeuchi, JHEP **1206**, 108 (2012).
  - [20] G. Klamke and D. Zeppenfeld, JHEP **0704** (2007) 052.
  - [21] C. Ruwiedel, N. Wermes and M. Schumacher, Eur. Phys. J. C **51**, 385 (2007).
  - [22] M. R. Buckley and M. J. Ramsey-Musolf, JHEP **1109**, 094 (2011).
  - [23] for additional channels see *e.g.* S. Berge, W. Bernreuther and J. Ziethe, Phys. Rev. Lett. **100**, 171605 (2008).
  - [24] J. M. Butterworth, A. R. Davison, M. Rubin and G. P. Salam, Phys. Rev. Lett. **100**, 242001 (2008).
  - [25] J. Ellis and D. S. Hwang, JHEP **1209**, 071 (2012).
  - [26] L.F. Landau, Dok. Akad. Nauk USSR **60** (1948) 207; C.N. Yang, Phys. Rev. **77** (1950) 242.
  - [27] K. Hagiwara, S. Ishihara, R. Szalapski and D. Zeppenfeld, Phys. Rev. D **48**, 2182 (1993); K. Hagiwara, R. Szalapski and D. Zeppenfeld, Phys. Lett. B **318**, 155 (1993).
  - [28] D. L. Rainwater, D. Zeppenfeld and K. Hagiwara, Phys. Rev. D **59**, 014037 (1999); T. Plehn, D. L. Rainwater and D. Zeppenfeld, Phys. Rev. D **61**, 093005 (2000).
  - [29] N. Kauer, T. Plehn, D. Rainwater and D. Zeppenfeld, Phys. Lett. B **503**, 113 (2001).
  - [30] D. L. Rainwater and D. Zeppenfeld, JHEP **9712**, 005 (1997); J. R. Andersen, C. Englert and M. Spannowsky, arXiv:1211.3011 [hep-ph].
  - [31] J. Frank, M. Rauch and D. Zeppenfeld, arXiv:1211.3658 [hep-ph].
  - [32] K. Gottfried and J. D. Jackson, Nuovo Cim. **33**, 309 (1964); J. D. Jackson, J. T. Donohue, K. Gottfried, R. Keyser and B. E. Y. Svensson, Phys. Rev. **139**, B428 (1965).
  - [33] T. Han, D. Krohn, L. -T. Wang and W. Zhu, JHEP **1003**, 082 (2010).
  - [34] J. Alwall, D. Rainwater and T. Plehn, Phys. Rev. D **76**, 055006 (2007).
  - [35] A. Alboteanu, W. Kilian and J. Reuter, JHEP **0811** (2008) 010.
  - [36] K. Arnold, M. Bahr, G. Bozzi, F. Campanario, C. Englert, T. Figy, N. Greiner and C. Hackstein *et al.*, Comput. Phys. Commun. **180** (2009) 1661.
  - [37] E. Gerwick, T. Plehn and S. Schumann, Phys. Rev. Lett. **108**, 032003 (2012).
  - [38] J. Forshaw, J. Keates and S. Marzani, JHEP **0907**, 023 (2009); B. E. Cox, J. R. Forshaw and A. D. Pilkington, Phys. Lett. B **696**, 87 (2011).
  - [39] J. R. Andersen, T. Binoth, G. Heinrich and J. M. Smillie, JHEP **0802** (2008) 057; A. Bredenstein, K. Hagiwara and B. Jäger, Phys. Rev. D **77** (2008) 073004.
  - [40] J. Alwall, M. Herquet, F. Maltoni, O. Mattelaer and T. Stelzer, JHEP **1106** (2011) 128.
  - [41] N. D. Christensen, T. Han and Y. Li, Phys. Lett. B **693**, 28 (2010); D. Stolarski and R. Vega-Morales,

arXiv:1208.4840 [hep-ph].

- [42] W. -Y. Keung, I. Low and J. Shu, Phys. Rev. Lett. **101**, 091802 (2008).
- [43] K. Hagiwara, J. Kanzaki, Q. Li and K. Mawatari, Eur. Phys. J. C **56**, 435 (2008).
- [44] see e.g. V. M. Abazov *et al.* [D0 Collaboration], Phys. Rev. Lett. **104**, 241802 (2010).
- [45] N. D. Christensen and C. Duhr, Comput. Phys. Commun. **180**, 1614 (2009).
- [46] C. Degrande, C. Duhr, B. Fuks, D. Grellscheid, O. Mattelaer and T. Reiter, Comput. Phys. Commun. **183**, 1201 (2012); P. de Aquino, W. Link, F. Maltoni, O. Mattelaer and T. Stelzer, Comput. Phys. Commun. **183** (2012) 2254.
- [47] T. Junk, Nucl. Instrum. Meth. A **434** (1999) 435; T. Junk, CDF Note 8128 [cdf/doc/statistics/public/8128]; T. Junk, CDF Note 7904 [cdf/doc/statistics/public/7904]; H. Hu and J. Nielsen, in 1st Workshop on Confidence Limits, CERN 2000-005 (2000).